Toward a Demonstration of a Light Force Accelerometer

by

Krish Kotru

B.A, Tufts University (2008)

Submitted to the Department of Aeronautics and Astronautics
in partial fulfillment of the requirements for the degree of

Master of Science in Aeronautics and Astronautics

at the

MASSACHUSETTS INSTITUTE OF TECHNOLOGY

September 2010

Author .....
Department of Aeronautics and Astronautics
August 19, 2010

Certified by .....
Shaoul Ezekiel, Sc.D.
Professor of Aeronautics and Astronautics and
Electrical Engineering and Computer Science
Thesis Supervisor

Certified by .....
Richard Stoner, Ph.D.
Principal Member of the Technical Staff
Thesis Supervisor

Accepted by .....
Eytan H. Modiano
Associate Professor of Aeronautics and Astronautics
Chair, Graduate Program Committee

Toward a Demonstration of a Light Force Accelerometer

by

Krish Kotru

Submitted to the Department of Aeronautics and Astronautics
on August 19, 2010, in partial fulfillment of the
requirements for the degree of
Master of Science in Aeronautics and Astronautics

Abstract

The Light Force Accelerometer (LFA) is an optical inertial sensor in which radiation pressure from two counter-propagating laser beams optically confines a glass microsphere. Inertial acceleration of the device results in microsphere displacement along the sensitive axis, which is subsequently nulled by optical forces to provide an acceleration measurement. A simple calculation that takes into account fundamental noise processes in the LFA (i.e., shot noise and RIN in the laser beams) places the sensitivity limit of this accelerometer at < 100 ng. By incorporating widely available, inexpensive optical components into a simple design, a high-precision LFA could provide an appealing alternative to other sensors of comparable performance.

Previous work on the LFA revealed instabilities in proof mass position detection caused by the asphericity of microspheres. In this thesis, an alternative method for position detection which was less sensitive to shape-irregularities in microspheres was investigated. Results indicated that resolution of microsphere motion was enhanced significantly when the new detection method was implemented. This improvement, however, did not eliminate the position instabilities observed previously. Capabilities for optical trapping with two counter-propagating beams in air were also developed in this work. Trapping with feedback position control in air was demonstrated for the first time, but long-term trapping in vacuum was prohibitively difficult due to destabilizing mechanical vibrations. For a microsphere in atmospheric pressure, the estimated bias stability was 318 μg after 300 seconds of averaging, and the approximate short-term sensitivity was 500 $\mu g/\sqrt{\text{Hz}}$. Stabilization of mechanical vibrations and precise calibration of power measurements to acceleration will allow this two-beam trap to probe the performance limits of the LFA.

Thesis Supervisor: Shaoul Ezekiel, Sc.D.
Title: Professor of Aeronautics and Astronautics and
Electrical Engineering and Computer Science

Thesis Supervisor: Richard Stoner, Ph.D.
Title: Principal Member of the Technical Staff

Acknowledgments

It is hard to imagine how different the last two years of my life would have been had I not spent them at MIT and Draper Labs. Chances are I would have slept more, but in exchange for those restful hours I would have given up the wonderful opportunity to work with some of the most interesting and intelligent people I know. For this opportunity, and for the support over the past two years, I thank Dr. Richard Stoner and the Draper Fellowship program. I am also indebted to my fellow lab rat and good friend, Dave Butts, for his help with not only this thesis, but also just about every other important part of graduate school. To the rest of the group at Draper, in particular, Brian Timmons and Joe Kinast, thank you for making the lab a truly fun place to work. I would also like to thank Prof. Shauol Ezekiel for his helpful comments on this thesis and for his lighthearted approach to life, which has helped me keep things in perspective. Finally, I am grateful for my loving parents, my sister, my grandmother, and girlfriend, Allison, all of whom have been tremendously supportive of me in their own special way.

This thesis was prepared at the Charles Stark Draper Laboratory, Inc., under the Precise Inertial Sensing Internal Research and Development Contract CON05025-99 Project ID 24066 Activity ID 002.

Publication of this thesis does not constitute approval by Draper or the sponsoring agency of the findings or conclusions contained herein. It is published for the exchange and stimulation of ideas.

Krish Kotru

Assignment

Draper Laboratory Report Number T-1670.

In consideration for the research opportunity and permission to prepare my thesis by and at The Charles Stark Draper Laboratory, Inc., I hereby assign my copyright of the thesis to The Charles Stark Draper Laboratory, Inc., Cambridge, Massachusetts.

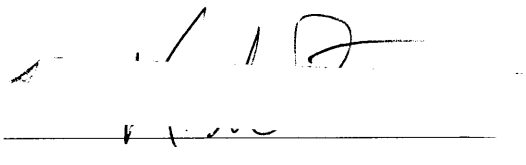

Krish Kotru

8/19/2010

Date

THIS PAGE INTENTIONALLY LEFT BLANK

Contents

1 Introduction **17**

1.1 Motivation for high-precision accelerometers 17

1.2 Introductory accelerometer concepts 18

1.2.1 Force-Rebalancing Accelerometers 19

1.2.2 Performance specifications 20

1.3 Historical origins and development 20

1.4 Optical Inertial Sensors 21

1.4.1 Overview of thesis 22

2 Optical Trapping **25**

2.1 Radiation Pressure 25

2.2 Forces in an optical trap 27

2.2.1 Theoretical calculation of optical forces 27

2.3 Dual-beam optical trap 29

2.4 Application to inertial sensing and other fields 31

3 Light Force Accelerometer Concept **33**

3.1 Optical Force-Rebalancing 33

3.2 Advantages of the LFA 34

3.2.1 Noise statistics 34

3.2.2 Real-time scale factor calibration 36

3.2.3 Simple, Compact, Solid-State Design 38

3.3 Concept Limitations 38

3.3.1 Asphericity in microspheres 38

3.3.2 Cross-axial coupling of proof mass motion 38
3.3.3 Trap initiation 39

4 Previous Experimental Work **41**
4.1 Signs of misshapen microspheres 41
4.2 Problems with imaging of misshapen microspheres 43
4.2.1 Large-angle reflection in microspheres 43
4.2.2 Small-Angle Refraction in microspheres 43
4.2.3 Optical tweezers for position detection 45

5 Experimental Apparatus **47**
5.1 Goals for experimental work 47
5.2 Overview of the Apparatus 47
5.2.1 Single-beam Levitation 47
5.2.2 Dual-beam Levitation 48
5.3 Collection Optics and Position Detection 49
5.4 PID Controller and Actuator 51
5.5 Details of the Components 52
5.5.1 Microsphere Proof Masses 52
5.5.2 Lasers 54
5.5.3 Current technique for trap initiation 55
5.5.4 Vacuum System 56

6 Experimental Results **57**
6.1 Overview of results 57
6.2 Small-angle refraction for optical position detection 58
6.2.1 Comparison of two position detection methods 58
6.2.2 Instability induced by misshapen spheres 60
6.3 Development of the dual-beam optical trap 62
6.3.1 Demonstration of trapping 62

6.3.2 Dual-beam trap in vacuum 65
6.4 Proof mass confinement through optical force-rebalancing 67
6.5 Performance Diagnostics 68
6.5.1 Short-term sensitivity 69
6.5.2 Bias stability 70

7 Conclusion **73**
7.1 Summary 73
7.2 Future Work 73

A Allan Variance **77**

THIS PAGE INTENTIONALLY LEFT BLANK

List of Figures

1-1 An idealized mass-spring system as an accelerometer. 18

1-2 Force-rebalancing, or closed-loop, accelerometer. Credit:[1]. 19

1-3 Bias stability and scale-factor stability for a wide range of accelerometers. Adapted from [2] 21

2-1 Transfer of light momentum via reflection and refraction in a dielectric. . . . 26

2-2 Left: Optical confinement of a microsphere situated at the beam waist. Right: A laterally displaced microsphere experiences a transverse restoring force. Adapted from [1] 28

2-3 Restoring transverse force generated by a tightly focused, 30 mW beam, incident on a 10 μm glass microsphere 29

2-4 Force diagram for a dual-beam optical trap 30

2-5 A perfectly aligned dual-beam trap in which there is no stabilizing force along the beam axis. 30

3-1 Optical force-rebalancing in the LFA. Top: Nominal operation when there is no input. Middle: Transient period in which an external force causes a shift in the microsphere position. Bottom: With $P_A > P_B$, microsphere position is restored to the set point. 35

3-2 A split photodetector measures microsphere position as deviations from the center of the detector. Credit: [1]. 36

3-3 Fundamental sensitivity limit of the LFA as a function of measurement interval. The demonstrated sensitivity of a cold-atom gravimeter is plotted for comparison. Credit: [3]. 37

3-4 Real-time scale factor calibration by dithering beam powers and measuring microsphere oscillations. Credit: [1]. 37
3-5 Graphical explanation of cross-axial coupling of microsphere motion 39

4-1 Top: Flat levitation beam power. Bottom: Microsphere position drifts over several seconds. Credit: [1]. 42
4-2 Allan deviation plot from previous results for a microsphere levitated with a single verticle beam in vacuum. Credit: [1] 43
4-3 Large-angle reflection of the levitation beam by the microsphere. Deformations perturb the optical signal used for position detection and contribute to instability. 44
4-4 Small-angle refraction of light from an illuminating beam. Refracted light should be less sensitive to asphericity in microspheres. 44

5-1 Schematic of single-beam levitation apparatus. Adapted from [1]. 48
5-2 The illuminating beam is directed toward the detector to create small-angle refraction. 49
5-3 Schematic of dual-beam trap apparatus. 50
5-4 Optics for imaging microspheres on a split photodetector when large-angle reflection is used for position control. 50
5-5 Optics for imaging microspheres on a split photodetector when small-angle refraction is used for position control. 51
5-6 FVOA time response to the edge of a square wave input 52
5-7 Logic of the control design for a dual-beam trap. This implementation provided constant power on a levitated microsphere, which minimized transverse motion. V_1 and V_2 are nominal offsets for each FVOA. 53
5-8 SEM photo of 1.5 μm fused silica microspheres. Credit: Corpuscular, Inc. . . 53
5-9 Apparatus for trap initiation. Resonances in the slide launch microspheres into the focus of the vertical beam. 55

6-1 Optics assembly that facilitated monitoring of microsphere motion with two detection methods, simultaneously. 58

6-2 Microsphere motion induced by oscillations in the trap initiation slide. Position detection based on refracted light visibly improves resolution. 59
6-3 Fourier transforms of position signals obtained simultaneously confirm resolution improvement. 60
6-4 Instability in single-beam levitation persists, particularly around the 10 second measurement interval. 61
6-5 Horizontal and vertical beam focusers are mounted on the same moveable surface. 63
6-6 Angular misalignments of the counter-propagating beams. Trapping is possible, nevertheless. 65
6-7 Left: 6 Hz oscillation in microsphere position in response to power oscillations at the same frequency in the horizontal beams. Right: Fourier transform of the position signal. 66
6-8 Amplitude response of the system over a range of 50 Hz. The system behaves like a double-integrator because of overdamping from air. 67
6-9 Position error signal for a stabilized microsphere. The motion is restricted to < 1 μm. 68
6-10 Time-series plot of data used for a short-term sensitivity calculation 70
6-11 Allan deviation of the dual-beam trap over a range of measurement intervals. The minimum Allan deviation at $\tau = 300$ sets the bias stability at 318 μg . . 71

7-1 Tilting of the accelerometer sensitive axis to apply a known acceleration input along the sensitive axis. 75

A-1 Method for computing the Allan deviation of a time-domain signal. 78

THIS PAGE INTENTIONALLY LEFT BLANK

Chapter 1

Introduction

1.1 Motivation for high-precision accelerometers

The ubiquity of GPS navigators in modern cars and cell phones has made navigation by external reference points a seemingly obvious concept. There is, however, a more basic navigation technique in which motion is tracked relative to a previous position. This displacement can be detected by continually measuring one's acceleration and orientation in the inertial reference frame, and using this information to calculate an evolving position and velocity.

Traditional inertial navigation systems (INS) employed this strategy using a combination of accelerometers, gyroscopes, and a simple computer. Accelerometers took linear acceleration measurements in three orthogonal directions while resting on a gyroscopically-stabilized platform, which maintained a fixed orientation with respect to an inertial reference frame. Together, these sensors comprised the inertial measurement unit (IMU). Measurements from the IMU were then integrated by the onboard computer to calculate velocity and position. In a modern INS, the accelerometers are commonly "strapped down" to the vehicle being navigated, and computers use rotation measurements from gyros to calculate the orientation of the body in the inertial coordinate system. Since all these operations are performed internally, inertial navigation, in principle, requires no external references.

In practice, position corrections (from GPS, for example) are incorporated because of the high sensitivity of inertial navigation to measurement errors. This sensitivity is illus-

trated by fact that an accelerometer with a 0.01 m/s^2 measurement offset, operating without correction for one hour, accumulates a position error of about 65 km. External corrections solve this problem, though they can be a luxury in hostile environments, bad weather, and periods of signal occultation. A more reliable option is to build a high-performance inertial sensor, which accumulates small errors. Such sensors have existed for decades and play important roles not only in navigation, but also in geophysical research, including seismology, oil prospecting, and gravimetry. State-of-the-art cold atom sensors, for instance, have measured gravity accurately to one part per billion [4].

1.2 Introductory accelerometer concepts

Typical accelerometers consist of three building blocks: A case, an object of known mass, and a physical mechanism that resists relative motion between the case and object. Together, these components measure the acceleration of the case in inertial space. A simple example is an idealized, frictionless mass-spring system shown on the left side of figure 1-1. Springs

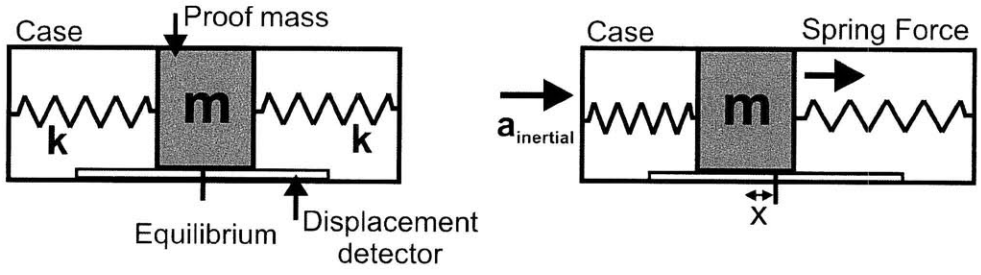

Figure 1-1: An idealized mass-spring system as an accelerometer.

connect the object of known mass—also called a proof mass—to the case, and a detector sits at the springs' equilibrium position. When the case is accelerated to the right, as shown on the right side of figure 1-1, the inertia of the proof mass initially causes a compression and stretching of the springs. The resulting spring force eventually overcomes the inertia and drives the proof mass to the same inertial acceleration as that of the case. Since

$$ma_{inertial} = F_{spring} = -2kx \tag{1.1}$$

a measurement of x, the displacement of the proof mass in the accelerometer reference frame, determines the acceleration of the case. In summary, an accelerometer senses its inertial acceleration by measuring the inertial force exerted on its proof mass.[1]

1.2.1 Force-Rebalancing Accelerometers

Open-loop accelerometers, such as the mass-spring sensor in figure 1-1, incorporate a displacement measurement into a model of the system dynamics to calculate specific force. In another class of accelerometers, specific force is determined by measuring the force needed to actively pin a proof mass to a fixed position in the accelerometer reference frame. An example of these closed-loop, or force-rebalancing, accelerometers is shown in figure 1-2. External forces acting on the accelerometer case cause the magnetic pendulum to swing away from equilibrium. This deviation is sent to a controller, which supplies the necessary current to the forcing magnetic coils to cancel the motion of the pendulum. Acceleration is then determined by monitoring the current that passes through the coils.

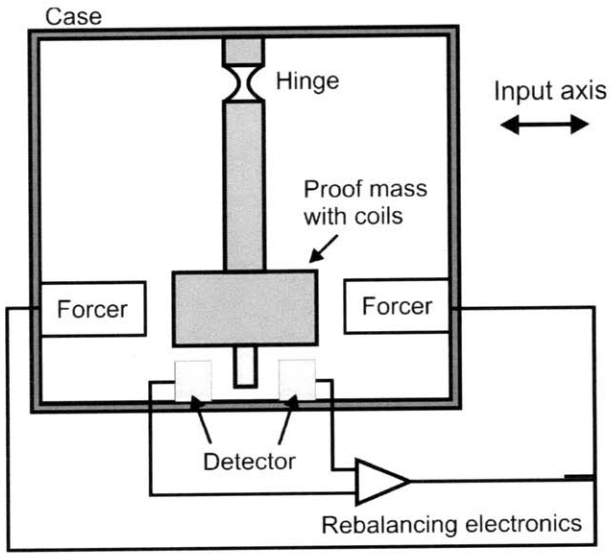

Figure 1-2: Force-rebalancing, or closed-loop, accelerometer. Credit:[1].

Since proof mass motion is restricted in a closed-loop configuration, nonlinearities re-

[1]More accurately, accelerometers measure specific force, defined as $S = a_{inertial} + g$. Gravity equally and simultaneously accelerates the proof mass and case of an accelerometer; the lack of relative motion makes the accelerometer blind to gravity. In practice, gravitational offsets are accounted for with gravity maps and gravimeters.

lated to position detection and system dynamics are easily avoided. For this reason, force-rebalancing accelerometers can withstand stronger accelerations and offer higher levels of precision than their open-loop counterparts.

1.2.2 Performance specifications

The performance attributes of an accelerometer can vary widely from one design to another, and are crucial in selecting the appropriate sensor for a given application. Some of the more frequently cited accelerometer specifications include bias stability, scale factor stability, sensitivity, and maximum input. Bias is the non-zero measurement taken by a sensor receiving zero acceleration input. Even the most accurate accelerometers have small biases due to manufacturing errors and other subtle effects. Since biases change over time (leaving no simple way to remove them), the stability of the bias over varying time intervals is used to determine the period over which the measurement provides the highest precision. Scale factor is the ratio of accelerometer output to input; the extent to which this ratio drifts in response to changes in the environment or the sensor itself is characterized by scale factor stability. Finally, sensitivity is a measure of the smallest input an accelerometer can resolve through various noise processes.

1.3 Historical origins and development

The first practical accelerometer was part of a "black box" navigator that provided primitive trajectory control for the German V-2 rockets during World War II. Since then, inertial sensor development has primarily been driven by the desire for increasingly precise and accurate inertial navigation systems in military applications and space exploration. During the Apollo missions, for example, NASA contracted what was at the time a state-of-the-art INS that incorporated a digital computer. The system was designed by MIT's Instrumentation Laboratory[2], the leading American innovator of inertial navigation technologies during the Cold War. While ground-based measurements played the principal navigation role in Apollo, inertial measurements remained necessary for verifying data from the ground and for traversing the dark side of the moon [5].

[2]Current the Charles Stark Draper Laboratory

Following Apollo, a paradigm shift during the 1970s drove inertial sensor development away from expensive, complex electromechanical instruments, and toward cost-effective, simpler equivalents [6]. Solid-state optical devices, such as the Ring Laser Gyro (RLG), used the interference of laser beams to measure rotation, while MEMS instruments introduced in the following decade facilitated previously unfathomable levels of miniaturization. MEMS-based accelerometers, which are currently found in consumer electronics such as smart phones, digital cameras, and video game controllers, tend to be economical, compact, and easily bulk-manufactured, though not especially precise. Figure 1-3 shows a variety of accelerometers that have been organized in terms of their bias stability and scale factor stability.

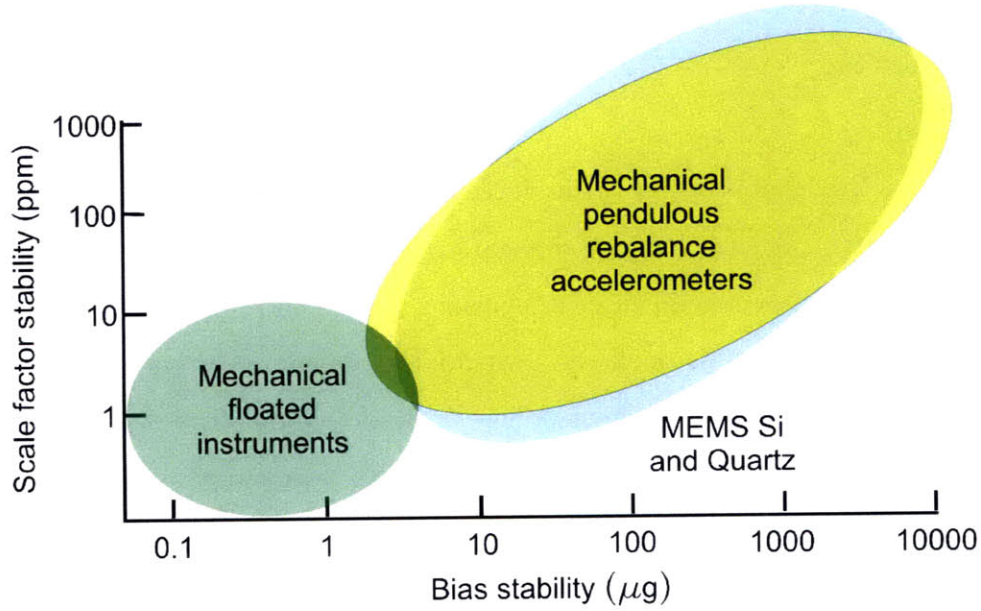

Figure 1-3: Bias stability and scale-factor stability for a wide range of accelerometers. Adapted from [2]

1.4 Optical Inertial Sensors

A purely optical inertial sensor uses the interference of light to sense motion. The appropriate geometry for measuring linear acceleration is a Michelson interferometer. Light from the source is split in perpendicular directions and then reflected back toward a detector by mirrors located at the ends of each interferometer arm. When the interferometer is accelerated parallel to one of the arms, the path length of the corresponding beam is lengthened during

travel in the forward direction and shortened upon return. The difference between the path lengths of each beam creates a relative phase shift that can be detected as a change in total power on an optical power detector.

A Michelson interferometer configuration was applied in a fiber optic accelerometer developed in the 1980s. In this device, a laser beam is divided between two fibers of equal length, one of which is adjoined to a mass. Accelerations cause the mass to stretch the attached fiber, creating a path length difference that changes the relative phase of the two beams. This accelerometer has demonstrated micro-g sensitivities in laboratory experiments, and is currently used in shock measurement applications [7].

The subject of this thesis is the Light Force Accelerometer (LFA): A novel accelerometer concept consisting of two counter-propagating laser beams whose optical forces confine a free-floating glass microsphere in three dimensions. Unlike most optical inertial sensors, the LFA does not exploit interference effects. Instead, the optical forces are used to actively cancel inertial forces that displace the microsphere in the accelerometer reference frame, making the LFA a force-rebalancing accelerometer. As a simple technology based on standard optical components and a solid-state design, the LFA may achieve high levels of precision while limiting the cost and complexity associated with comparable sensors.

1.4.1 Overview of thesis

This thesis builds on previous demonstrations of fundamental functions in the LFA, such as optical confinement of microspheres and optical force-rebalancing. In particular, it investigates the effects of misshapen microspheres on position detection and describes the development of microsphere levitation with counter-propagating beams. Chapter 2 describes the origins of optical forces on microspheres and details the mechanics of the two-beam trap, which is central to an LFA. In chapter 3, the concept of optical force-rebalancing in the LFA is presented, and known advantages and limitations are discussed. Chapter 4 presents relevant results from previous developments of fundamental capabilities for an LFA, such as

optical levitation in high-vacuum and optical force-rebalancing. The discussion is focused on observations from that research, and their influence on the directions taken in this thesis. The details of the experimental apparatus used in this work, including descriptions of lasers, microspheres, and electro-optic components, are presented in chapter 5. In chapter 6, experimental results relating to the resolution of microsphere position and the demonstration of a counter-propagating beam trap in air and with position stabilization are presented. Preliminary performance specifications, namely bias stability and short-term sensitivity, are also included. The thesis is concluded in chapter 7, in which we give a summary of results and suggestions for useful work in the future.

THIS PAGE INTENTIONALLY LEFT BLANK

Chapter 2

Optical Trapping

2.1 Radiation Pressure

Radiation pressure is the transfer of momentum from light to another object. As an example, consider a ray of light with momentum $\mathbf{p}$ that reflects off an initially stationary mirror. We assume normal incidence so that, for simplicity, the momentum of the reflected ray is -$\mathbf{p}$. So far, this system violates conservation of momentum because its initial and final momentums differ by $2\mathbf{p}$. The mirror, however, is also part of the system and balances the conservation equation by acquiring a final momentum of $2\mathbf{p}$. If the mirror is replaced with an opaque object, the incident ray is absorbed rather than reflected. To conserve momentum, the object gains momentum $\mathbf{p}$ because the ray ceases to exist in the final state of the system. The last case of interest is when the ray impinges on a dielectric material at an off-normal angle. As shown in figure 2-1, 40% of the light is reflected and 60% is transmitted (assuming there is no absorption). The dotted arrows on the dielectric side of the boundary are the momentum vectors of the reflected and refracted rays when the dielectric is not present. $\Delta\mathbf{p}_r$ and $\Delta\mathbf{p}_t$ represent the redirection of these momentum vectors by the surface. As a result, the dielectric gains a momentum of $-\Delta\mathbf{p}_t + -\Delta\mathbf{p}_r$ to satisfy the conservation law.

It is now clear that, in principle, radiation pressure can influence the motion of an object. Creating this motion in microscopic objects requires, a laser beam, which provides high levels of optical power over a small area. The momentum per second, or optical force F, in a laser

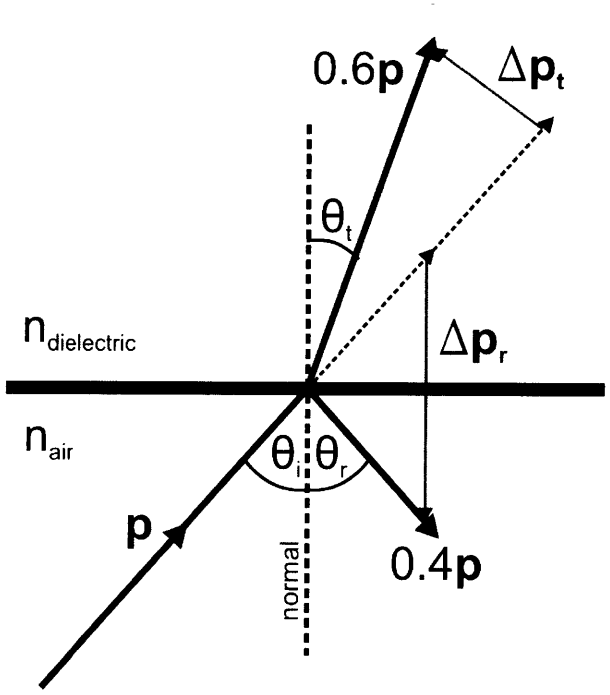

Figure 2-1: Transfer of light momentum via reflection and refraction in a dielectric.

beam is given by the equation

$$F = \frac{P}{v} = \frac{nP}{c} \tag{2.1}$$

where P is the power of the beam, v is its speed, c is the speed of light in vacuum, and n is the refractive index of the surrounding medium. Based on this equation, a 100 mW laser beam in air produces about 300 pN of optical force, which is certainly enough to move a micro-sized object when the beam is of comparable width.

After performing a similar back-of-the-envelope calculation in the late 1960s, physicist Arthur Ashkin of Bell Laboratories demonstrated the effects of radiation pressure by accelerating a 2 μm latex sphere, suspended in water, with a Gaussian laser beam. Surprisingly, the beam also confined the sphere transversely, indicating that an optical force perpendicular to the beam axis was present [8]. By adding an identical counter-propagating beam, which cancelled the axial force on the sphere, Ashkin demonstrated the first all-optical trap [9]. Since the trapping forces described here are central to the LFA, we devote the next section to an examination of their origins.

2.2 Forces in an optical trap

When a dielectric sphere with high relative index is placed in a Gaussian beam, it experiences optical forces that accelerate it along the beam axis and confine it transversely. The origins of these forces are best understood by dividing the beam into constituent rays and calculating the momentum transferred to the sphere by their reflection and transmission components.[1] Consider one such ray with power P, traveling through a medium with refractive index n_1 and impinging on a glass sphere with index $n_2 > n_1$. A fraction R of the incident power forms a reflected ray, where R is the reflectance of the glass and the remaining fraction T forms a transmitted ray. Since the vast majority of light incident on a glass sphere is transmitted, forces due to reflection can be excluded for brevity [11]. In passing, we note that reflection assists primarily in accelerating the sphere along the beam axis[2].

To isolate refraction effects, the left side of figure 2-2 depicts the transmission components of two rays that impinge symmetrically about the sphere. Refraction at the top and bottom faces of the sphere results in the indicated optical forces. Because these forces are symmetric, they cancel in the transverse direction and accelerate the sphere in the axial direction. This symmetry is broken, however, when the sphere is displaced laterally within the beam, as shown in the right side of figure 2-2. Since ray 1 carries more power than ray 2, F_1^i and F_1^o overpower F_2^i and F_2^o and pull the sphere back to the beam axis. Note that the transverse stabilizing force enables optical trapping if a downward axial force from gravity or a second laser beam is added to the picture.

2.2.1 Theoretical calculation of optical forces

To calculate the force exerted by a laser beam on a sphere, the beam is divided into constituent rays. The forces from these rays are then further broken into axial and transverse components. In the literature, the axial component is referred to as scattering force and the transverse component is called gradient force—we will adhere to this nomenclature from

[1] This geometric optics approach is valid if the sphere diameter is equal to many wavelengths of the light. Smaller spheres require Rayleigh scattering or Mie theory treatments, the details of which can be found in reference [10]

[2] The reader is referred to [1] for a complete discussion

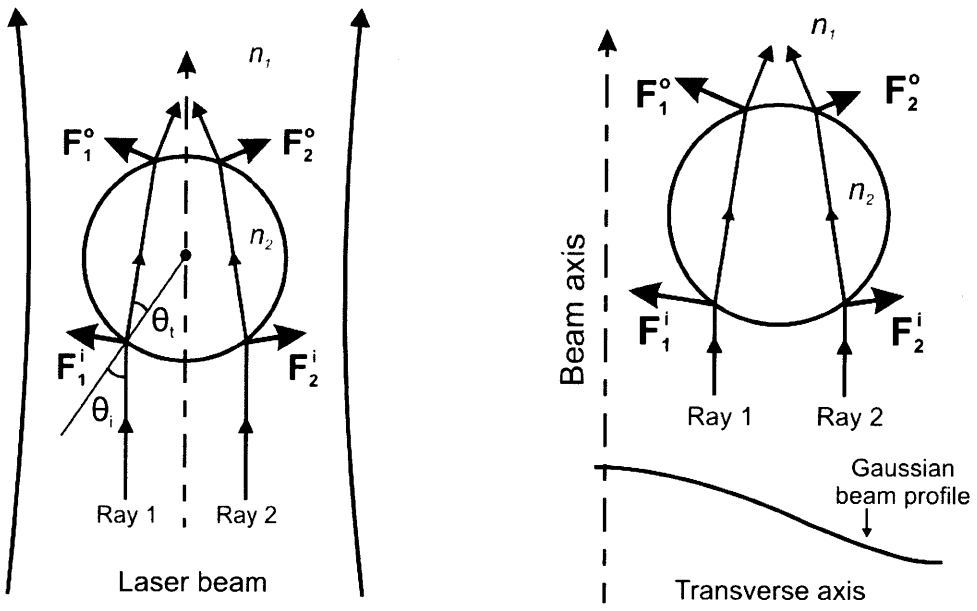

Figure 2-2: Left: Optical confinement of a microsphere situated at the beam waist. Right: A laterally displaced microsphere experiences a transverse restoring force. Adapted from [1]

here on. These perpendicular components can be represented as

$$F_{scat} = Q_s \frac{n_1 P}{c} \tag{2.2}$$

$$F_{grad} = Q_g \frac{n_1 P}{c} \tag{2.3}$$

where the efficiencies, Q_s and Q_g, are functions of the incidence angle and the indices of refraction. Exact closed-form expressions for the efficiencies, which even take into account the infinite number of reflections occurring within the sphere, have been reported [12, 13]. With these expressions, the force contributions from the rays are calculated and summed to determine the gradient and scattering forces exerted by an entire beam. Figure 2-3 shows the result of this calculation when a 30 mW beam, focused to 10 μm at the waist, is incident on a 10 μm glass sphere. The shape of this curve clearly indicates that F_{grad} opposes transverse motions of the sphere.

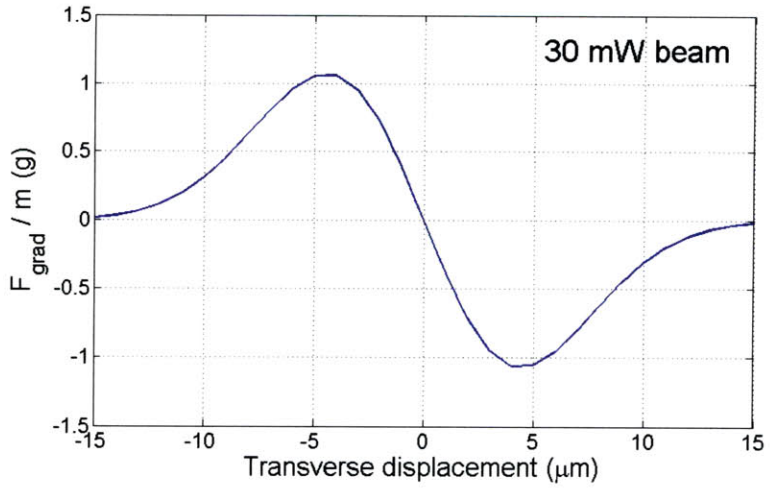

Figure 2-3: Restoring transverse force generated by a tightly focused, 30 mW beam, incident on a 10 μm glass microsphere

2.3 Dual-beam optical trap

The first demonstrated all-optical trap, discussed in section 2.1, is conceptually identical to the trap used in the LFA. In this trap, two focused, counter-propagating beams, shown in figure 2-4, optically confine a dielectric sphere at a stable equilibrium point between the beam waists. At the equilibrium point, the scattering forces from each beam, $F_{\text{scat,A}}$ and $F_{\text{scat,B}}$, are equal, and the force due to gravity is balanced by the sum of the gradient forces, $F_{\text{grad,A}}$ and $F_{\text{grad,B}}$. The equilibrium position is stable because if the sphere moves downward, the gradient forces increase and accelerate the sphere back toward its starting position. Furthermore, if the sphere shifts to the left, it receives a larger portion of beam A than of beam B, implying that $F_{\text{scat,A}}$ overpowers $F_{\text{scat,B}}$. As a result, the sphere is pushed toward the equilibrium point with an acceleration this is proportional to $F_{\text{scat,A}} - F_{\text{scat,B}}$. Experiments with dual-beam optical trapping in air revealed that the stability of an equilibrium point is, in general, dependent on the ratio of sphere radius to beam width [14]. In the relevant case where this ratio is < 1, the above description applies.

When the beam waists of a dual-beam trap are separated, the net scattering force resists the axial motion of the sphere like a spring. This restoring force is necessary for stable optical trapping in an open-loop system. In a closed-loop accelerometer, however, sensitivity to

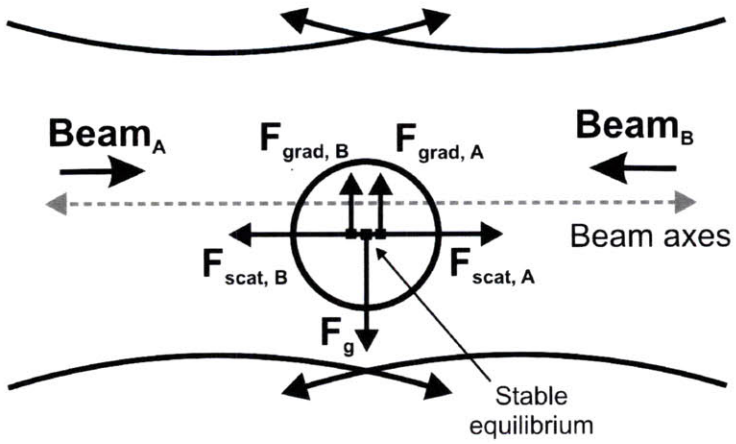

Figure 2-4: Force diagram for a dual-beam optical trap

inertial inputs is improved when there is no restoring force (i.e. the proof mass is completely free along the sensitive axis). An idealized example of a dual-beam trap that exerts no restoring force is shown in figure 2-5. Since the beams are confocal and of identical shape and power, their scattering forces cancel over the entire beam axis. In practice, this configuration is approximated using beams with Rayleigh ranges that are many proof mass diameters. Such beams are nearly collimated in the trapping region, implying that their scattering forces do not change drastically for small displacements in the beam axis.

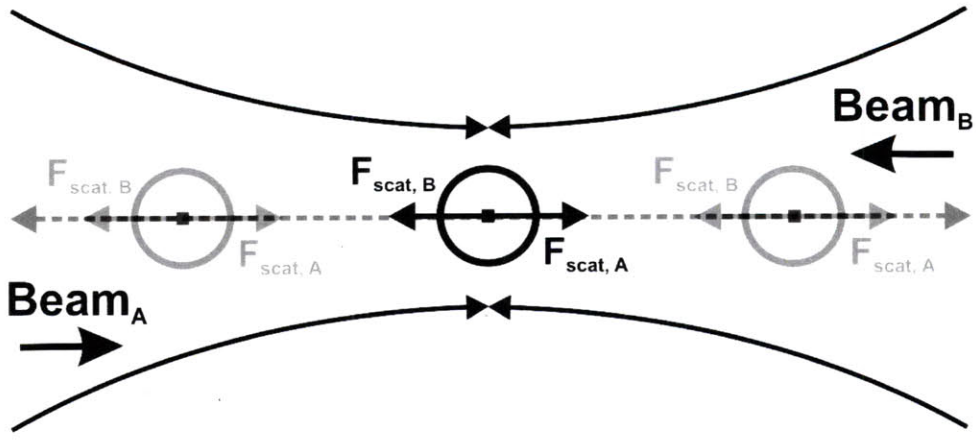

Figure 2-5: A perfectly aligned dual-beam trap in which there is no stabilizing force along the beam axis.

2.4 Application to inertial sensing and other fields

An optically confined sphere in high-vacuum experiences virtually no resistance to motion, making it a nearly free proof mass for an accelerometer. Ashkin himself noted the applicability of optical techniques to inertial sensors when he wrote, "If the viscous damping (from air) can be further reduced, applications to inertial devices such as gyroscopes and accelerometers become possible" [15]. Given the tremendous reductions in the size and cost of laser and vacuum technology over the decades, a deployable optical sensor based on optical trapping is no longer purely fantasy.

Optical trapping techniques have also been significantly refined through their widespread use in biology and atomic physics. A trap called optical tweezers, for example, has helped biologists initiate cell fusion in a controlled manner and measure forces from enzymes that interact with DNA during RNA transcription [11]. A tweezers trap consists of one highly convergent beam that confines an object in any orientation [16] [13]. In the realm of atomic physics, counter-propagating beams have been used to cool atomic vapors to micro-Kelvin temperatures in a technique called "optical molasses" [17] [11].

THIS PAGE INTENTIONALLY LEFT BLANK

Chapter 3

Light Force Accelerometer Concept

A dual-beam optical trap, as described in chapter 2, uses two focused, counter-propagating beams to levitate a spherical dielectric bead. One could hypothetically use this passive trap as an open-loop accelerometer, much like the mass-spring sensor described in chapter 1. In that example, a simplistic model of spring dynamics and measurements of proof mass displacement determined inertial acceleration. Applying such a model to the dual-beam trap, however, would be prohibitively complex due to beam shape, proof mass heating effects, and large displacements, amongst other things. Because of these complications, a closed-loop approach is applied in the LFA. This method and its anticipated advantages and limitations are explored in this chapter.

3.1 Optical Force-Rebalancing

In the LFA, a dual-beam optical trap senses inertial input by using optical forces to actively restrict the motion of a microsphere proof mass. The top level diagram in figure 3-1 shows the LFA just before an external force is applied to its case. Since there is no inertial input, the beam powers, P_A and P_B, are equal and the proof mass remains motionless. When the external force is added, there is a transient period in which the inertial acceleration of the case creates a corresponding proof mass displacement (in the accelerometer reference frame). This displacement is nulled by an imbalance in the beam powers that provides an inertial acceleration to the proof mass. A position feedback loop controls this imbalance, which effectively alters the relative strength of the opposing scattering forces, $F_{\mathrm{scat,A}}$ and $F_{\mathrm{scat,B}}$,

while maintaining constant gradient force.[1] Since inertial acceleration is proportional to power difference, the beam powers can be measured and differenced to determine acceleration [18].

Force-rebalancing is triggered by deviations in proof mass position, which can be detected using levitation light reflected by the microsphere. This light is focused on a split photodetector, whose top and bottom sections record separate power signals, as depicted in figure 3-2. The difference between these signals, which is referred to as error, provides a measure of microsphere deviation from the set point—typically the position that centers the image on the detector. Additionally, the difference signal is normalized by the sum, making it less sensitive to fluctuations in the beam powers. Without this modification, the error signal would change in response to drift in the total power (proportional increases in A and B), even if the microsphere were motionless.

Proof masses for the LFA typically have micron-scale diameters to limit the optical power necessary for trapping. At atmospheric pressure, frequent collisions between a small proof mass and gas molecules (Brownian motion) generate a persistent jitter in microsphere position that reduces short-term sensitivity. This problem is solved in the LFA by trapping microspheres in an evacuated vacuum chamber so that the surrounding pressure level is below 1 mTorr.

3.2 Advantages of the LFA

3.2.1 Noise statistics

One inherent advantage to optical force-rebalancing is its low-noise statistics. In an idealized picture of the LFA, the two laser beams are generated from the same laser, carrying common-mode intensity noise that cancels perfectly when there is no inertial input and the beam powers are matched. The fundamental sensitivity limit, assuming the proof mass is in high vacuum, is shot noise in the laser, which results from spontaneous photon emissions and affects intensity as well as trajectory.

When inertial inputs are present, the beam powers are no longer equal and relative

[1] This minimizes transverse motion due to a constant gravitational input in a laboratory experiment

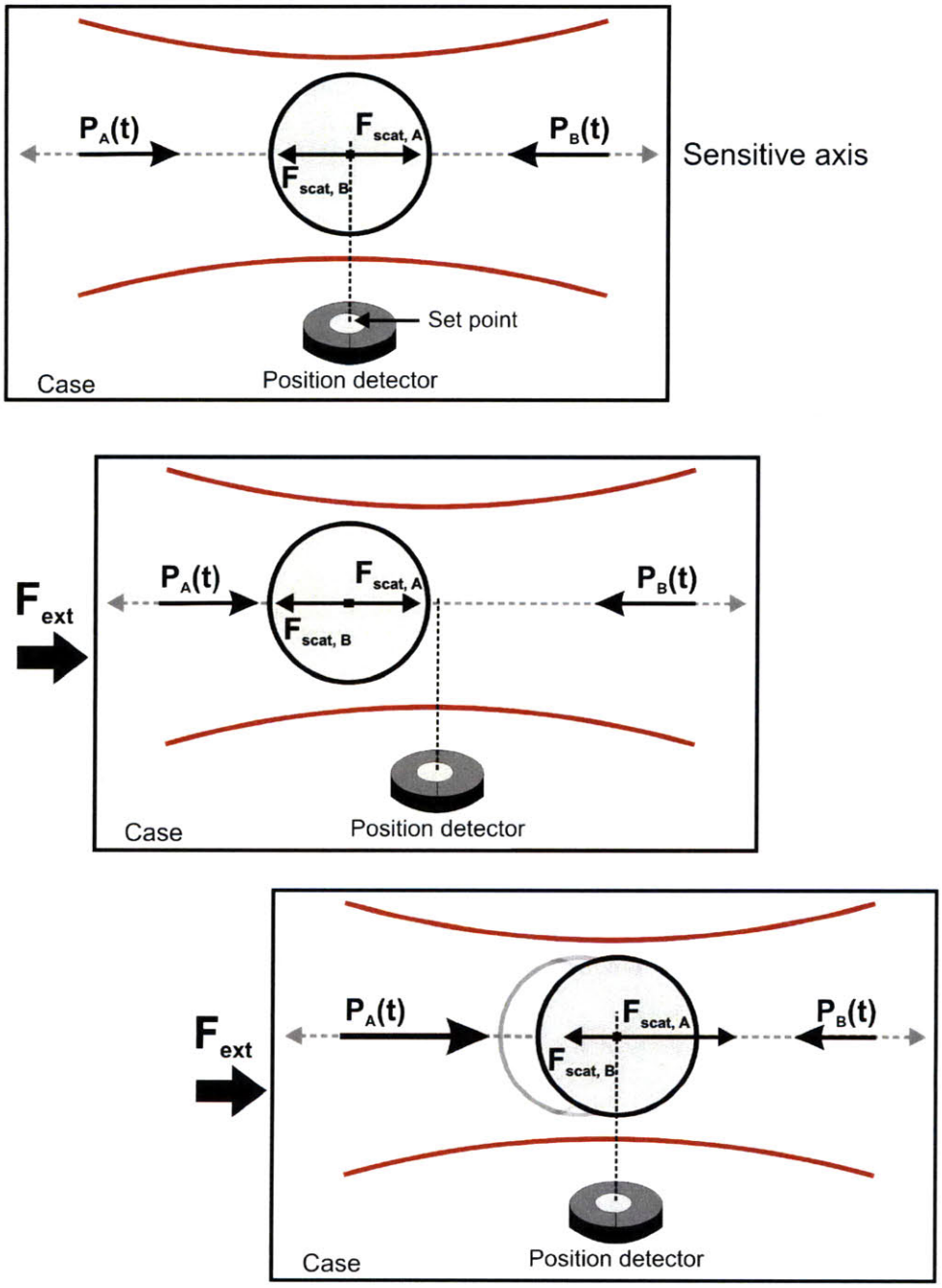

Figure 3-1: Optical force-rebalancing in the LFA. Top: Nominal operation when there is no input. Middle: Transient period in which an external force causes a shift in the microsphere position. Bottom: With $P_A > P_B$, microsphere position is restored to the set point.

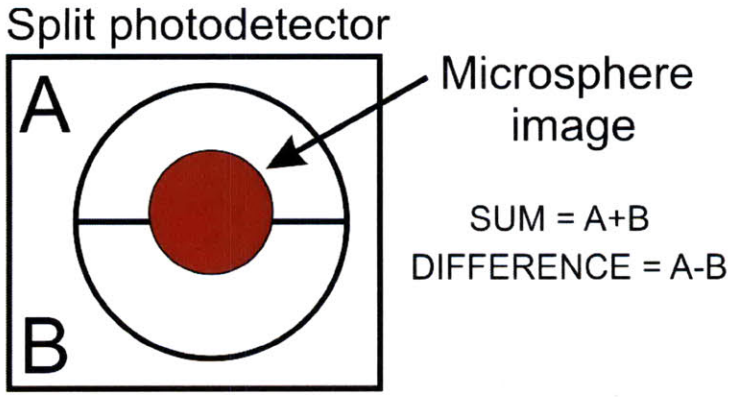

Figure 3-2: A split photodetector measures microsphere position as deviations from the center of the detector. Credit: [1].

intensity noise (RIN) in the laser becomes an important noise source. In an analogous situation, a single vertically oriented beam balances the weight of a microsphere in closed-loop, effectively producing a 1 g inertial input. Analysis of the noise statistics of this system, excluding all other biases, reveals that the RIN noise decreases as $1/\tau$, where τ is the time over which the acceleration measurement has been averaged [3].[2] As shown in figure 3-3, the sensitivity limit drops down to the ng level after 10 seconds of averaging. Given the relative simplicity of the LFA and the intricacy of other high-precision sensors, this device would be valuable even if its practical realization only achieved μg sensitivities.

3.2.2 Real-time scale factor calibration

The measurement of interest in the LFA is the power difference between the counter-propagating beams, which determines acceleration through a proportional calibration. This calibration, or scale factor, can change over time if, for example, there are variations in the level of vacuum, the shape and relative orientation of the beams, or the size of the sphere due to heating.

The scale factor K can, in principle, be calibrated in real-time by incorporating a sinusoidal power dither of opposite signs and amplitude δP in each of the beams, as shown in figure 3-4. The resulting oscillation in microsphere position at frequency ω is described by the dynamics of simple harmonic motion, $K\delta P = w^2\delta x$, assuming there is negligible air

[2]Readers unfamiliar with the Allan Variance a referred to appendix A for a brief explanation of this statistic.

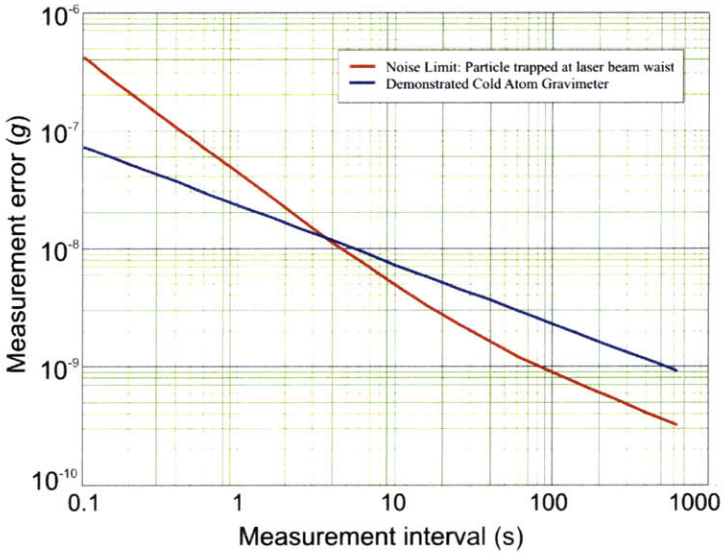

Figure 3-3: Fundamental sensitivity limit of the LFA as a function of measurement interval. The demonstrated sensitivity of a cold-atom gravimeter is plotted for comparison. Credit: [3].

damping in a high vacuum environment. If the power dither is applied at a frequency above the bandwidth of the control loop, but within that of the detector, the scale factor can be determined without affecting the acceleration measurement.

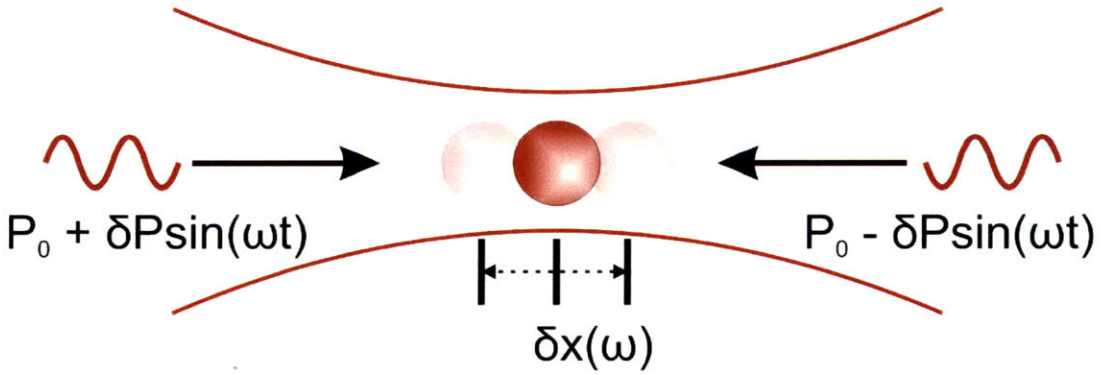

Figure 3-4: Real-time scale factor calibration by dithering beam powers and measuring microsphere oscillations. Credit: [1].

3.2.3 Simple, Compact, Solid-State Design

Many fundamental capabilities for an LFA were demonstrated in the 1970s, but a simple and compact design nevertheless remained out of reach. Forty years later, reductions in the size and cost of modern high-power lasers, electro-optics, and optical fiber have brought a realistic design well within the realm of possibility. The current bench-top design of the LFA, for example, uses inexpensive and widely available components (the vast majority of which are solid-state constructions) in an assembly that requires little beyond the precise alignment of the trapping beams.

3.3 Concept Limitations

3.3.1 Asphericity in microspheres

The discussion of the LFA so far has assumed proof masses to be perfectly spherical and uniform, when in truth, deformities have a significant effect on trap dynamics. Misshapen spheres receive an asymmetrical distribution of forces from the optical trap, resulting in motion which affects bias stability in unpredictable ways. Irregular spheres also can affect microsphere position detection by creating light fields that are uncorrelated to real motion. In this case, it is apparent motion that degrades instrument performance. Previous experiments, however, have recorded maximum deviations in microsphere position of < 1 μm in open-loop traps, indicating a high spherical quality can be achieved [12].

3.3.2 Cross-axial coupling of proof mass motion

Open-loop gradient forces help create a stable optical trap by limiting the range of transverse microsphere motion. But without active transverse position control a number of problems arise. If the LFA experiences a constant inertial input in the transverse direction, the microsphere finds an off-axis equilibrium point, thereby changing the scale factor since a larger fractional power imbalance is need for stabilization. A more troubling situation occurs when the LFA experiences a transverse jolt while receiving a constant axial input. In figure 3-5, ΔF_{axis} initially balances the constant axial force, but the addition of a transverse input moves the microsphere to the beam tails. The net scattering force at this radial position, ΔF_{tail}, is

too weak to balance the original input, thereby producing axial microsphere motion and an apparent acceleration in the sensitive axis.

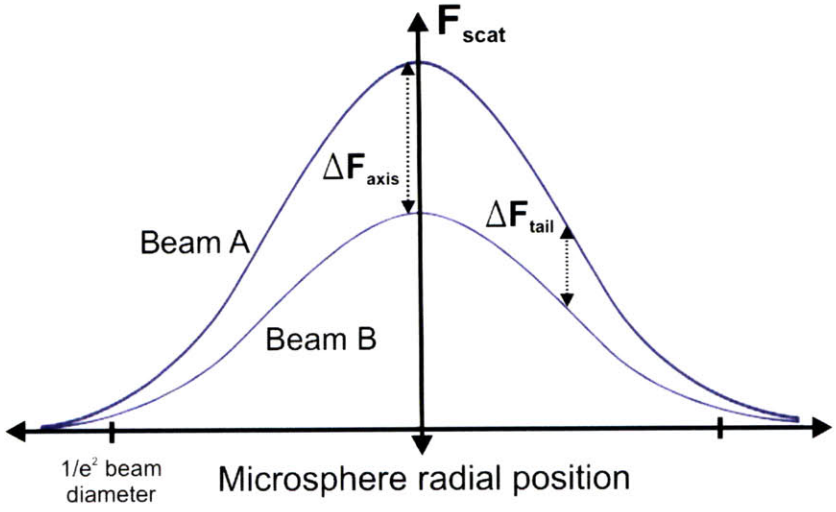

Figure 3-5: Graphical explanation of cross-axial coupling of microsphere motion.

Closing the loop on radial microsphere motion is conceptually similar to the axial case. Since the sum of the beam powers is proportional to the gradient force, a second control loop can adjust the sum to actively pin the microsphere to the beam axis. Transverse and axial control can be decoupled, because the sum and difference of the powers are independent of each other. Changes in the total optical power may introduce biases related to heating, but these effects operate at much longer time constants than those caused by uncorrelated proof mass motion.

3.3.3 Trap initiation

The automated placement of microspheres into an optical trap is an engineering problem currently lacking a reliable solution. The difficulty relates to the tendency of microspheres to amass and stick to surfaces through Van der Waals interactions that strongly overpower optical forces. Large microspheres suppress the sticking force, but also raise the minimum optical power needed for levitation. The sphere size used in the current trap initiation technique achieves a balance between these opposing effects. The initiation technique, however, is user-intensive and would be difficult to either automate or extend to 0 g and high-vacuum environments (the details behind this technique are presented in chapter 5). In its final

incarnation, the LFA will ideally be capable of immediately and automatically replacing a microsphere that has been ejected from the high-vacuum optical trap, thus minimizing the accelerometer "blackout" period.

Chapter 4

Previous Experimental Work

In its early stages, development of the LFA focused on demonstrating fundamental capabilities, such as optical trapping of microspheres in vacuum, and position stabilization of a proof mass [1]. A dual-beam optical trap was not a prerequisite for this work. A simpler alternative was to use a single vertically oriented beam to levitate a microsphere against the force of gravity, as done in Ashkin's experiments with optical levitation [15]. Feedback control was included by adjusting the power of the levitation beam so that the height of the microsphere was locked to the set point established by a split photodetector [19, 20].

Since the work in this thesis builds upon these previous experiments, the relevant results are presented in this chapter to provide a clear context for the steps that followed.

4.1 Signs of misshapen microspheres

The single-beam LFA successfully demonstrated the basic capabilities for an LFA listed earlier. In the process, these demonstrations revealed significant fluctuations in the microsphere position signal that were uncorrelated with the levitation beam power. The data in figure 4-1, for example, show the position signal for a microsphere levitated in open-loop, and a concurrent trace of the beam power. The circled position drifts display accelerations as large as 400 μg , which are unaccounted for by the 0.01% fluctuations in the power signal. This percent change amounts to < 100 μg of acceleration when the mean beam power is taken to be approximately 1 g. A more likely source for these drifts was asphericity in the proof mass. Qualitative observations of the levitated sphere revealed changing light fields that cor-

responded to the drifts in figure 4-1 [1]. As discussed in the previous chapter, asymmetries in the optical forces acting on a misshapen sphere can initiate rotations and wobbles, as well as apparent motion in the split detector.

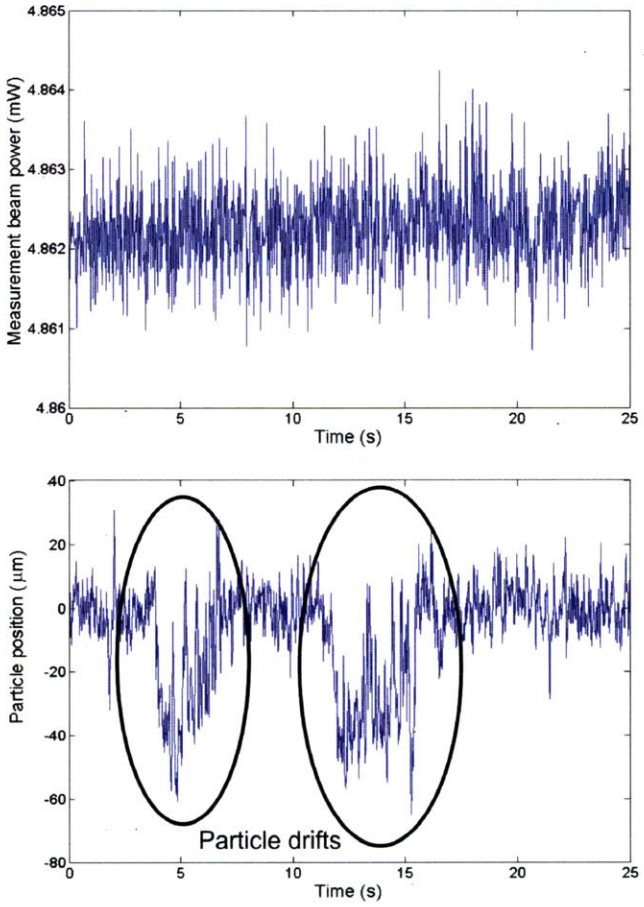

Figure 4-1: Top: Flat levitation beam power. Bottom: Microsphere position drifts over several seconds. Credit: [1].

The Allen deviations of the optical power in the single-beam LFA, plotted in figure 4-2, show the time intervals over which different noise processes diminished stability. The flattening of the curve around the 10 second measurement interval suggests biases with durations of several seconds affected the acceleration measurement. This time scale corresponds well with those of the position drifts observed in figure 4-1, providing further evidence that these motions were a significant source of bias instability [1].

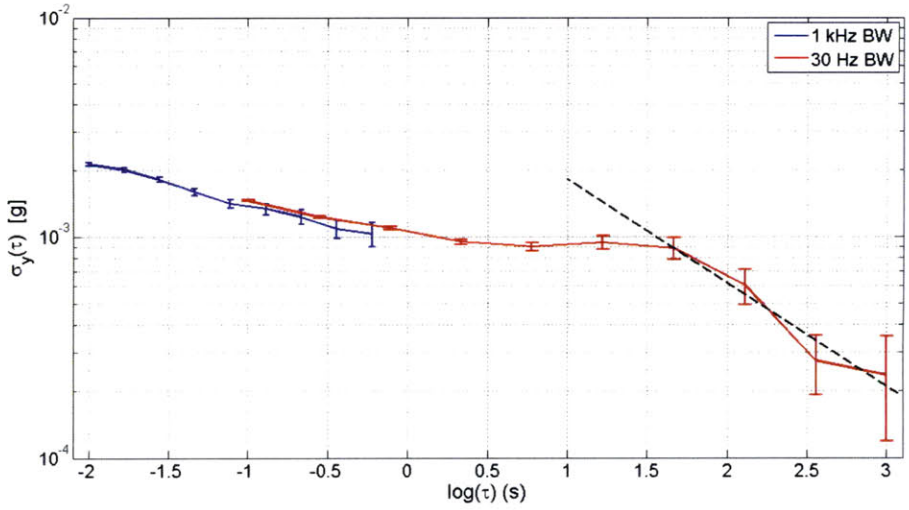

Figure 4-2: Allan deviation plot from previous results for a microsphere levitated with a single verticle beam in vacuum. Credit: [1]

4.2 Problems with imaging of misshapen microspheres

4.2.1 Large-angle reflection in microspheres

The bias instability in the result discussed above suggests the position detection method may have been overly sensitive to asphericity. In the single-beam LFA, position detection relied on a microsphere reflecting light from the levitation beam perpendicular to the beam axis. The solid arrows in figure 4-3 trace the nominal path taken by light rays that reach the split detector. Before exiting the sphere, the light undergoes a large-angle internal reflection that makes the remainder of the path sensitive to redirection by deformations of the microsphere surface. An exaggeration of this effect is represented by the dotted red arrow in figure 4-3. In practice, the non-uniformly reflected light from a misshapen sphere rotates like a lighthouse, causing a time-varying redirection of the path.

4.2.2 Small-Angle Refraction in microspheres

An alternative position detection method minimizes vulnerability to surface anomalies by imaging light refracted at small angles. As shown in figure 4-4, a separate laser beam, prop-

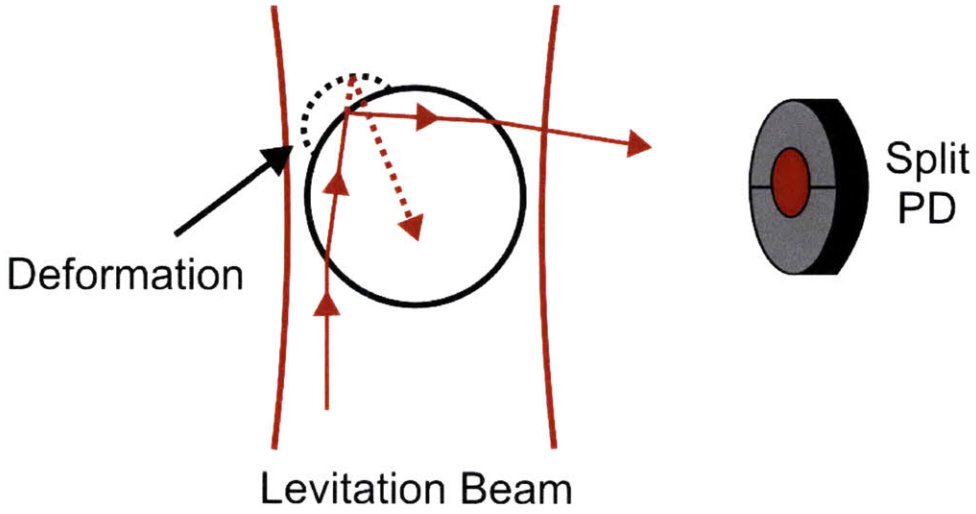

Figure 4-3: Large-angle reflection of the levitation beam by the microsphere. Deformations perturb the optical signal used for position detection and contribute to instability.

agating directly towards the detector, illuminates the levitated sphere. Light that reaches the detector after passing through the sphere experiences small-angle refraction, creating a path that is deflected at a smaller angle by aspherical surface features.

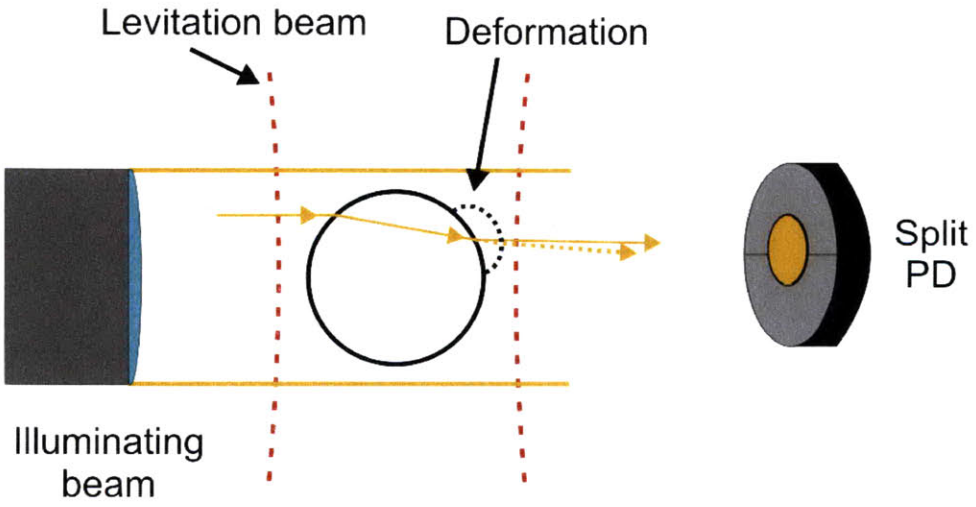

Figure 4-4: Small-angle refraction of light from an illuminating beam. Refracted light should be less sensitive to asphericity in microspheres.

The illuminating beam biases the acceleration measurement because it exerts optical forces on the sphere transverse to the levitation beam, and causes motion along the sensitive axis through cross-axis coupling. This effect can be made negligible by selecting a beam

intensity such that the force on the microsphere is much smaller than the forces imparted by the levitating beam. The illuminating beam should be orders of magnitude wider than the microsphere diameter to provide illumination over a large range of motion and nearly uniform intensity in the vicinity of the sphere. Uniform intensity can also be produced by a top-hat beam, which requires more complex optics. Choosing different wavelengths for the levitation and illumination beams permits filtering of the large-angle reflected light from the trapping beam, thereby avoiding undesired proof mass images. Finally, light that does not pass through the sphere can be obscured to prevent the refracted light from being washed out. The next chapter describes an assembly of simple optics that serves this purpose.

While the small-angle refraction method suppresses the effect of a distorted light field on the position measurement, it does not eliminate actual motion caused by surface irregularities. Therefore, this method will only reduce the types of biases seen in previous work if their source was apparent motion.

4.2.3 Optical tweezers for position detection

The two position detection methods considered in this work are only sensitive to motion in two dimensions. In a deployable LFA, three-dimensional position detection may be necessary if the active control of transverse microsphere motion is desired. A third method for position detection, which senses motion in all three axes, uses optical tweezers to illuminate the microsphere. Because tweezers traps use tightly focused beams, proof mass motion over a small range of the illuminating beam axis changes the total power reaching the split detector linearly [21]. Apparatus refinements discussed in reference [21] may yield a linear response over a 2 μm range of motion. The necessary sensitivity to total power in the position signal implies that power drifts in the illuminating beam would have to be controlled by a feedback loop. Additionally, the narrow width of the illuminating beam would limit the detectable range of motion, though this would not matter in a sensitive device that strictly confined microsphere position.

THIS PAGE INTENTIONALLY LEFT BLANK

Chapter 5

Experimental Apparatus

5.1 Goals for experimental work

The primary goals of this thesis were to

1. investigate and improve the measurement of proof mass position for feedback control
2. develop a dual-beam optical trap that would enable characterizations of accelerometer performance (e.g., bias stability and sensitivity)

Since microsphere position measurement is, in theory, independent of the trapping geometry, the first objective was approached with an existing setup for single-beam levitation. This apparatus provided stable optical trapping and was easily expanded with a dual-beam trap, which accomplished the second goal. The experimental apparatus is described in detail in this chapter.

5.2 Overview of the Apparatus

5.2.1 Single-beam Levitation

In single-beam microsphere levitation, scattering forces from a vertically oriented beam balanced the weight of the sphere and gradient forces provided transverse confinement. Transforming this optical trap into an inertial sensor required closed-loop levitation, as depicted in figure 5-1. Light from the levitation beam, reflected perpendicular to the beam axis by the

sphere, was imaged on a split detector. When the microsphere deviated from its set point, the detector produced an error signal for an analog controller, which is described later in this chapter. The controller applied a tuning voltage to a variable optical attenuator, which adjusted the levitation beam power and returned the sphere to the set point.

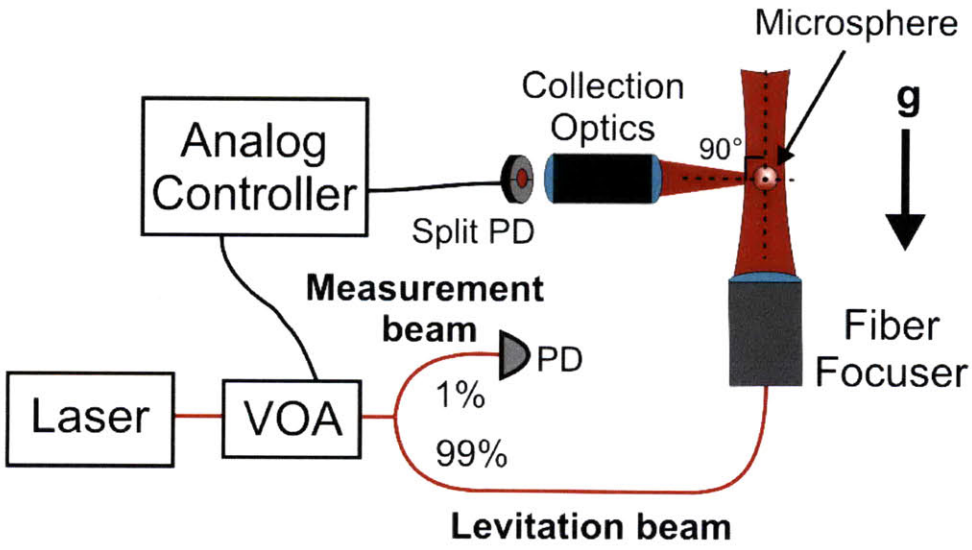

Figure 5-1: Schematic of single-beam levitation apparatus. Adapted from [1].

The acceleration of the sphere was proportional to the total optical power of the beam. To measure acceleration, 1% of the beam was directed to a photodetector via optical fiber, yielding a power measurement whose mean value was proportional to 1 g. Fractional variations in power about the mean value were then calibrated in gs.

Microsphere position detection was also accomplished by illuminating the sphere with a separate laser beam, as shown in figure 5-2. The orientation of this beam with respect to the detector guaranteed small-angle refraction by the sphere and made the detection system less sensitive to shape irregularities. See chapter 4 for a detailed discussion of this technique.

5.2.2 Dual-beam Levitation

The dual-beam optical trap used two focused, counter-propagating, horizontally oriented laser beams to levitate a microsphere, as illustrated by the top-down view of the apparatus in figure 5-3. In this trap, the sum of the gradient forces levitated the sphere against gravity and the difference in scattering forces provided lateral stability. A measurement of microsphere

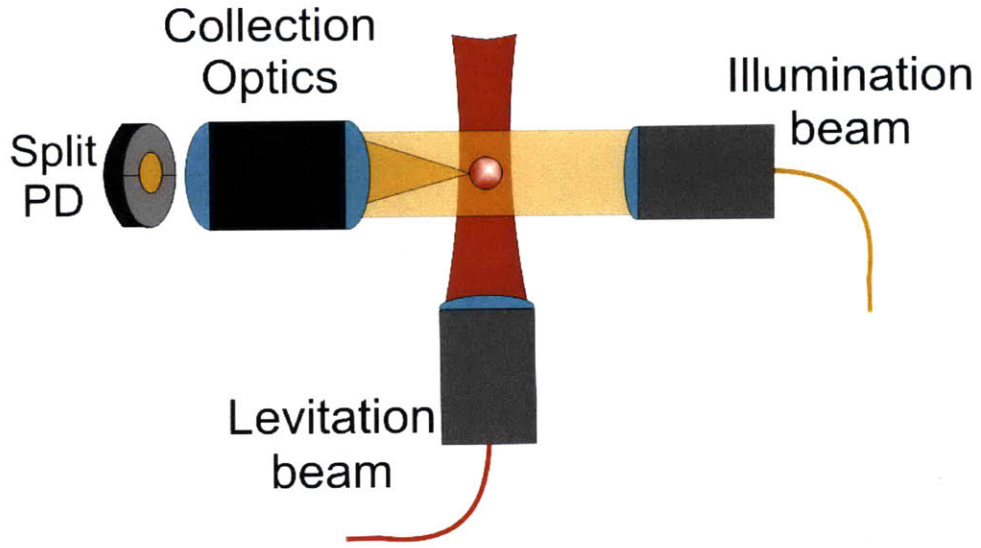

Figure 5-2: The illuminating beam is directed toward the detector to create small-angle refraction.

position was obtained through the large-angle reflection method (though, in principle, either position detection method could have been used). An analog controller received the position error signal and adjusted the power balance between the beams accordingly.

5% to 10% of the power from each levitation beam was picked off in free-space by sample covers (150 μm in thickness) and directed to photodetectors, providing measurements of the beam powers. Differencing the beam powers yielded a quantity proportional to acceleration. However, because the mean power difference corresponded to 0 g, these measurements had to be calibrated to acceleration through an experiment discussed in the next chapter.

5.3 Collection Optics and Position Detection

Position detection of any kind required light from the microsphere to be collected, magnified, and imaged on a split detector. Figure 5-4 illustrates the collection optics used in the large-angle reflection technique for position detection. Light reflected by the microsphere was passed through a 2-f imaging system, which created a 1:1 image of the microsphere in front of a 10x microscope objective. After passing through the microscope, the magnified light field was directed on to a silicon split photodetector.[1] The resulting normalized error signal

[1]New Focus Quadcell Photoreceiver, Model 2901.

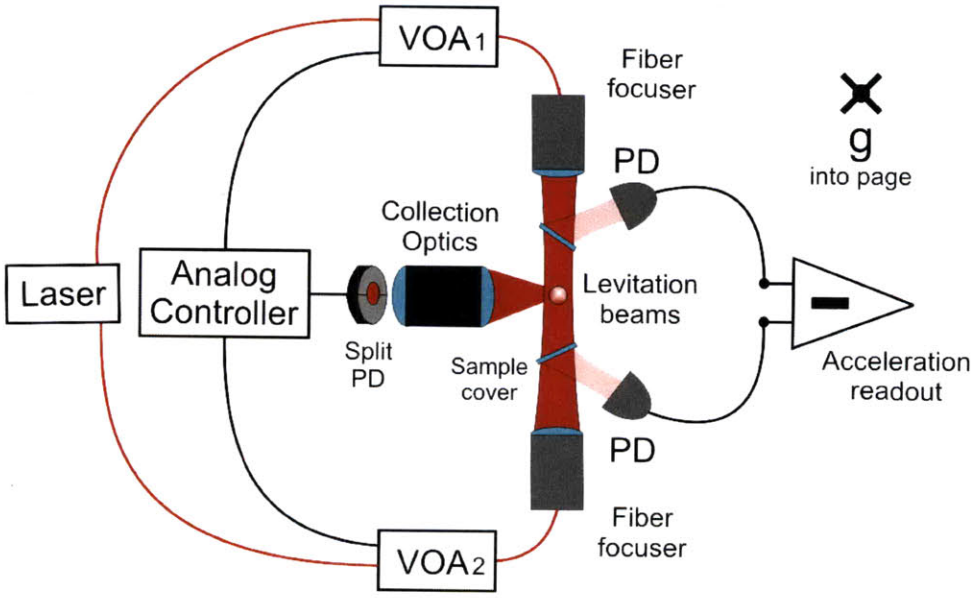

Figure 5-3: Schematic of dual-beam trap apparatus.

provided a measure of microsphere motion that mitigated the effects of power fluctuations in the levitation beam. These electronics had a 100 kHz bandwidth.

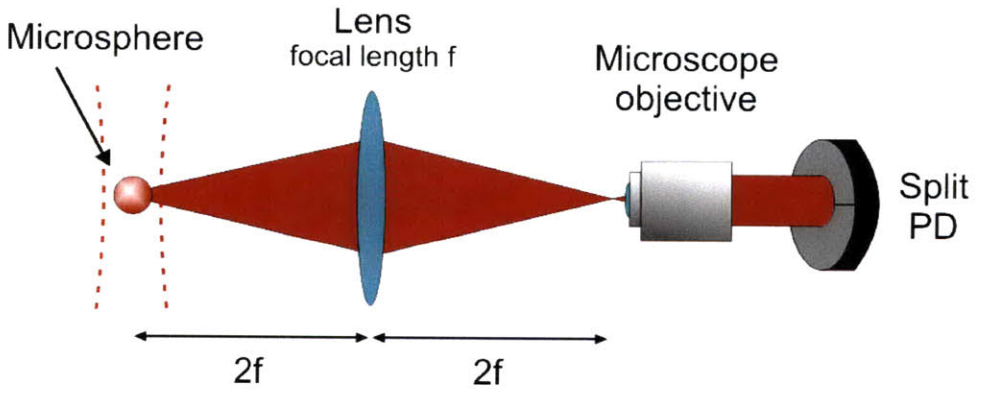

Figure 5-4: Optics for imaging microspheres on a split photodetector when large-angle reflection is used for position control.

In the small-angle refraction method, the cross-sectional area of the illuminating beam was 10,000 times larger than that of the microsphere. Therefore, light passing around, rather than through, the sphere had to be discarded to prevent the refracted light from being washed out. The collection optics illustrated in figure 5-5 accomplished this task. Non-refracted light remained part of the collimated illuminating beam, and was focused

by the first converging lens on to a small beam block, fashioned out of a 1.5 mm spot of Aquadag[2] on a glass microscope slide. The first lens was chosen with a focal length roughly equal to its distance from the sphere, thereby nearly collimating the refracted light. With the beam block occluding a negligible fraction of this light, a second converging lens focused the light on to a 10x microscope objective. Finally, the enlarged spot was bandpass filtered and then imaged on a custom, InGaAs split photodetector (700 Hz bandwidth).

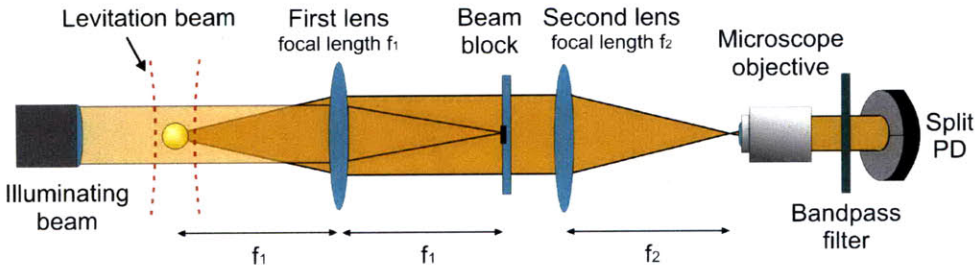

Figure 5-5: Optics for imaging microspheres on a split photodetector when small-angle refraction is used for position control.

5.4 PID Controller and Actuator

Position feedback control in the single-beam trap was achieved by sending the error signal from the split photodetector to an analog PID controller[3]. In addition to the typical proportional, integral, and derivative tuning parameters, the controller also had a roll-off option that set the bandwidth to 3 kHz. The integral, derivative, and roll-off time constants were all lowered by a factor of 100 for higher bandwidth control, because the original design was intended for large-scale temperature regulation.

Correction signals were sent to a MEMS fast variable optical attenuator (FVOA)[4], which provided rapid, stable modulation of the levitation beam power. The MEMS package contained a piezo-actuated rotation stage that supported a mirror. As the applied voltage varied, the mirror rotated and altered the coupling between the input and output fibers, providing a maximum attenuation of 30 dB. Rotation speed was tested by applying a square wave voltage input with an amplitude of 5 V to the FVOA (in practice, the maximum rated

[2]Aquadag is a black, colloidal dispersion of graphite in water, which sticks to most surfaces
[3]Linear Research Inc., Model LR-130.
[4]DiCon FiberOptics Inc., Richmond, CA.

input of 10 V was never needed). The plot in figure 5-6 shows the FVOA response to the leading edge of one of the square waves. The mirror rotated through the majority of its full range in 300 μs, and did not limit the position control bandwidth.

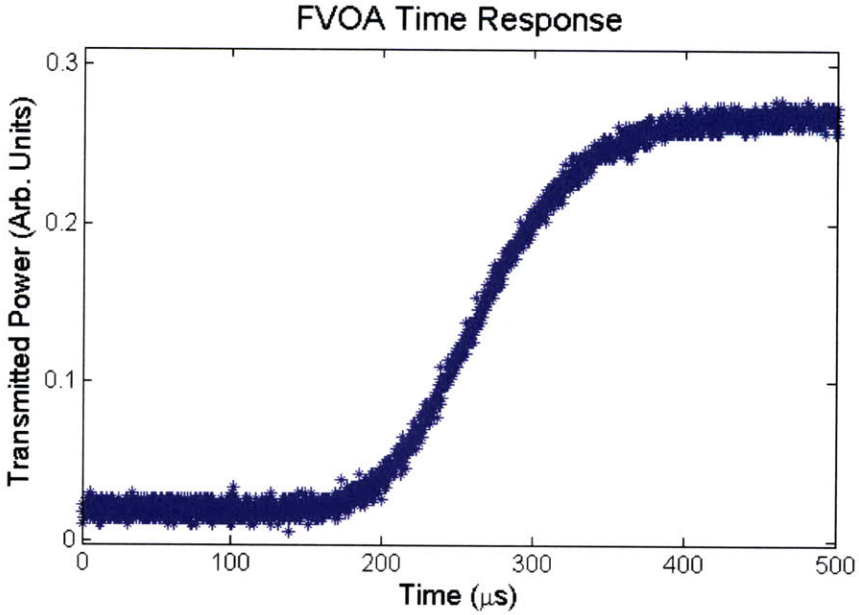

Figure 5-6: FVOA time response to the edge of a square wave input

In the dual-beam trap, feedback control was achieved with a modified version of the system described above. The error signal from the split photodetector was sent to the same PID controller, but the resulting control signal was electronically divided between two FVOAs, as shown in figure 5-7. Therefore, instead of leaving one beam at a constant power and modulating the other, both beams were modulated with opposing signs and equal magnitude to preserve the total power incident on the sphere. This design avoided undesired transverse motions due to fluctuating gradient forces.

5.5 Details of the Components

5.5.1 Microsphere Proof Masses

Pure fused-silica microspheres, 10 μm in diameter[5], were used as proof-masses because of their spherical quality and low absorption coefficient at 980 nm, which reduced heating

[5]Microspheres were fabricated by Corpuscular Inc.

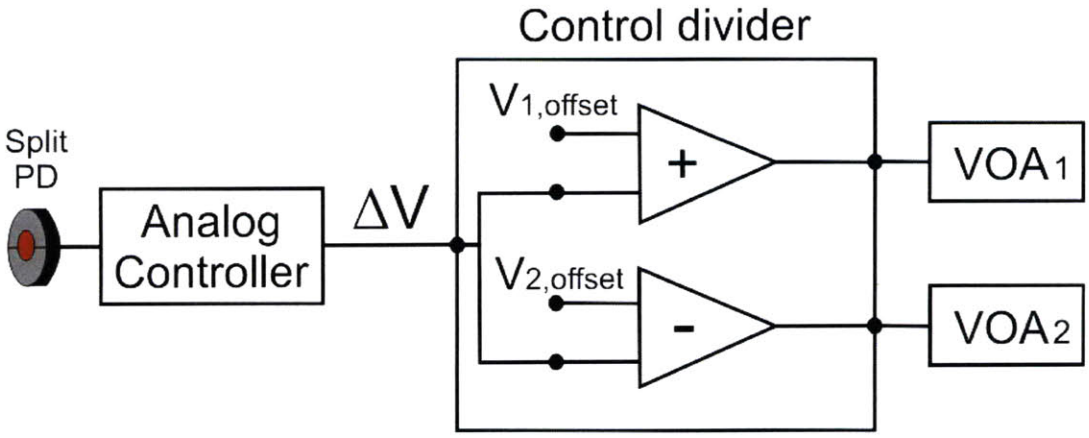

Figure 5-7: Logic of the control design for a dual-beam trap. This implementation provided constant power on a levitated microsphere, which minimized transverse motion. V_1 and V_2 are nominal offsets for each FVOA.

biases generated by the levitation beam.[6] The microsphere size was chosen as a compromise between the optical power needed to levitate a sphere, which scales as r^3, where r is the sphere radius, and Van der Waals forces, which cause particles to stick to each other and adjacent surfaces. Figure 5-8 shows fused silica microspheres of 1.5 μm diameters.

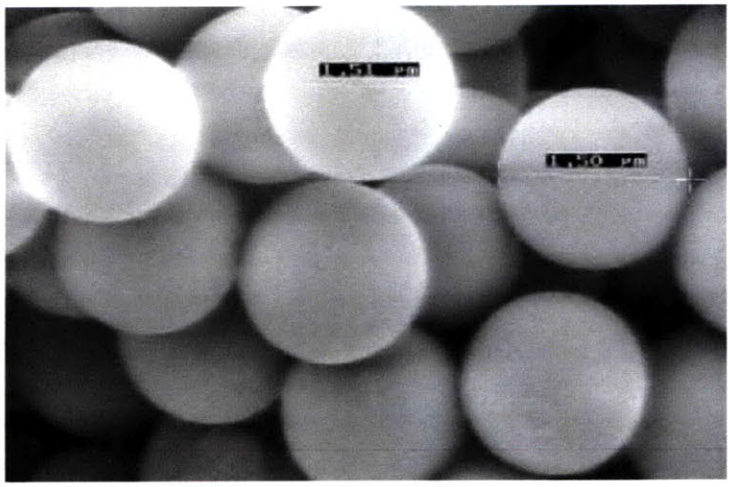

Figure 5-8: SEM photo of 1.5 μm fused silica microspheres. Credit: Corpuscular, Inc.

[6]The reader is directed to reference [1] for further detail.

5.5.2 Lasers

A Bookham 980 nm pump diode served as the light source for the vertical beam, supplying a maximum power of 300 mW when driven at a 400 mA current. Because of their ubiquity in the telecommunication industry, high-power laser diodes at this wavelength are widely available at low cost and over a range of power levels. Furthermore, common silicon CCD cameras are sensitive to 980 nm and provide the operator with valuable qualitative information, such as whether or not a microsphere has been steadily levitated.

The beam had a Gaussian intensity profile and was focused by a fiber-coupled focuser[7]. The focal length of the beam was 55 mm and its $1/e^2$ diameter at the waist was 10 μm, which ensured that 95% the light was incident on the particle. A low-noise current source and temperature controller[8] powered the laser and maintained a safe operating temperature. Vertical levitation was possible with a minimum beam power of 35 mW, but was normally done with 60 mW for higher stability.

A broadband 1550 nm source[9] generated the illumination beam used for small-angle microsphere position detection. Its fiber-coupled 100 mW output was launched into a 1 mm collimator[10]. At this power, the illuminating beam contributed approximately 20 μW of incident power to the microsphere, which was three orders of magnitude less than the optical force imparted by the levitation beam.

The horizontally oriented beams were produced by a second Bookham 980 nm pump diode with an output power of 600 mW at 950 mA of driving current. The single output from the pump was divided equally and directed through separate fiber focusers so that the resulting beams had 10 μm $1/e^2$ diameters at their waists, with 80 mm focal lengths. The laser was driven at a constant current by a low-noise ILX current source[11], which also monitored the temperature of the diode. Stable horizontal levitation was achieved with as little as 35 mW per beam, though typical powers were 90 mW per beam.

[7]OZ Optics Ltd.; focal lengths were accurate to $\pm 2\%$ of the spec.
[8]ILX Lightwave, models LDX-3620 and LDT-5525.
[9]Amonics Ltd., model ALS-C-20-B-FA.
[10]Oz Optics Ltd.
[11]ILX Lightwave, LDC-3744B.

5.5.3 Current technique for trap initiation

To place microspheres in the vertical levitation beam, many spheres were set on a microscope slide near the waist of the vertical laser beam, as shown in figure 5-9. Levitation, however, could not be achieved at this point because electrostatic forces stuck microspheres to the surface of the slide and overpowered the optical force from the laser beam. The sticking force was overcome by shaking the slide like a cantilever at a resonance frequency, which was near 29 kHz. Leaving one end of the slide free, the other end was attached to a piezo-actuated mount with epoxy[12]. Typically, the mount was shaken at a particular a mplitude and swept through a range of frequencies until a cantilever resonance was excited. The freed spheres then swarmed toward a vibration node in the slide, where the levitation beam was positioned. With the beam waist situated just above the slide, a moving sphere passing through the beam was lifted into a stable trap above the focus. Slide oscillations were then immediately halted to prevent other moving spheres from obscuring the beam.

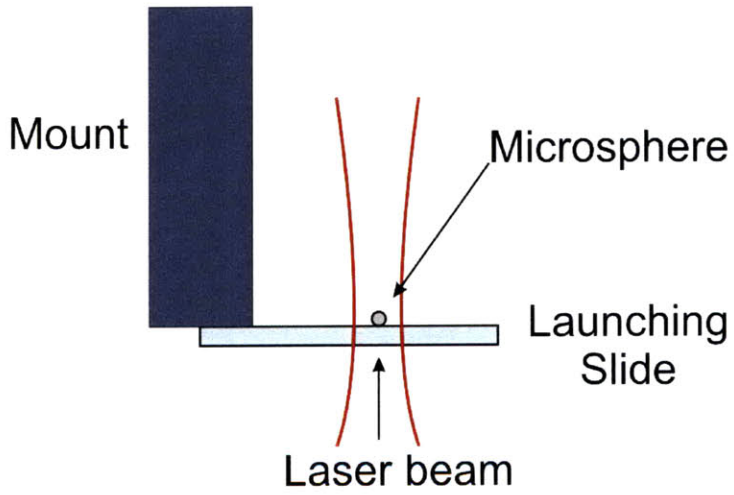

Figure 5-9: Apparatus for trap initiation. Resonances in the slide launch microspheres into the focus of the vertical beam.

Levitated microspheres were handed off to the dual-beam trap by raising the power of the vertical beam. If the trajectory of the vertical beam crossed near the equilibrium position of the dual-beam trap, the sphere could be elevated to a position where it became brightly illuminated by all three beams. The power of the vertical beam was then gradually reduced

[12]Stycast2741.

until the dual-beam trap captured the sphere. This hand-off technique was also implemented by Ashkin and Roosen in their work with dual-beam trapping in air [22, 14].

5.5.4 Vacuum System

As discussed in chapter 3, levitating microspheres in a high-vacuum environment is desirable because it maximizes short-term sensitivity in the LFA. Unfortunately, it also makes the initial trapping of microspheres virtually impossible due to the lack of damping from air drag. As a result, microspheres must initially be trapped in air before the surrounding pressure is lowered.

To accommodate this capability, levitation experiments were performed inside a small vacuum chamber[13] containing six viewports for optical access. The chamber was connected to a thermomolecular turbopump, a vacuum gauge[14] capable of sensing pressures from 0.1 Torr to 1 mTorr, and electrical feedthroughs for the piezos, all through UHV assembly components. Vacuum hardware connections were made with ConFlat flanges, which easily maintained adequate seals for the desired pressure level of < 1 mTorr. Destabilizing vibrations caused by the turbopump were suppressed by disconnecting any stiff links to the roughing pump, and an SAES getter pump helped maintain low pressure levels when the turbopump was disconnected.

[13] Kimball Physics Inc.
[14] Teledyne Hastings Instruments, model CVT-15AB.

Chapter 6

Experimental Results

6.1 Overview of results

This research built on previous demonstrations of fundamental capabilities for an LFA, such as optical trapping of microspheres in air and vacuum, and microsphere position stabilization using feedback control [1]. Observations from that work revealed that microsphere shape irregularities were contributing to instabilities in the optical trap, possibly by generating spurious position signals. Therefore, the investigation of an alternative method for position detection was a major focus of this thesis; the first set of results discussed in this chapter address this solution. The resolution of real microsphere motion was significantly improved with the alternative method. Results indicate, however, that the trapping instabilities were in fact unrelated to position detection.

The demonstration of a two-beam horizontal optical trap was the second primary goal of this thesis. This trap is stable regardless of its orientation, which is necessary for a deployable sensor. It additionally enables the characterization of any performance specification for an accelerometer, including constant bias since the inertial input is nominally 0 g along the sensitive axis. Preliminary bias stability and short-term sensitivity measurements for this system are presented in this chapter, along with a discussion of how these measurements were calibrated. Suggestions for future work and potential applications of this technology are covered in the following chapter.

6.2 Small-angle refraction for optical position detection

Microsphere position was detected in the LFA with two related techniques that were described in chapter 4. In the large-angle reflection method, light from the trapping beam, which was reflected perpendicular to the beam axis by the microsphere, was imaged on a split photodetector, as shown in figure 6-1 (this figure is discussed in the next section). The motions of the sphere were measured as deviations from a set point established by the detector. Alternatively, the small-angle refraction method used a separate laser beam, directed toward the split detector, to illuminate the levitated sphere. A small part of this beam was refracted by the sphere and imaged on a split detector. Since this image was less sensitive to shape irregularities in the microsphere, position measurement was expected to be better correlated with real motion.

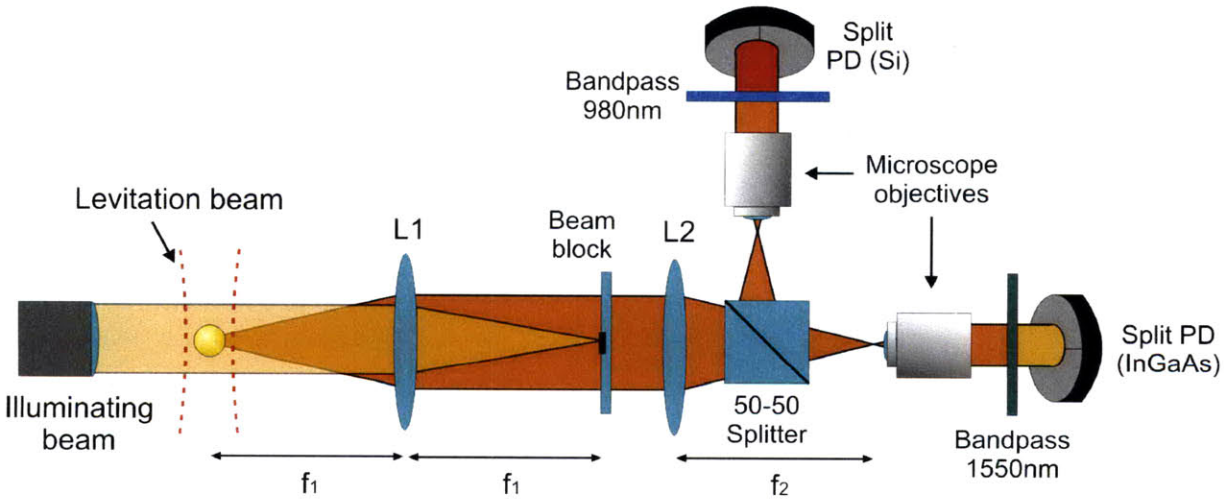

Figure 6-1: Optics assembly that facilitated monitoring of microsphere motion with two detection methods, simultaneously.

6.2.1 Comparison of two position detection methods

To experimentally compare the position detection methods, the deviations of a levitated microsphere were monitored with both techniques simultaneously. Since position measurement is independent of trap geometry, the simpler single-beam levitation apparatus was used to

levitate microspheres in open loop at atmospheric pressure. Simultaneous position detection was made possible by the combination of collection optics shown in figure 6-1. Reflected and refracted light from the microsphere effectively followed the same trajectory, which is indicated in the figure by the darker shade of orange. A 50-50 beam-splitting cube directed the light field toward two orthogonally positioned 10x microscope objectives. The light fields were then bandpass filtered so that the correct wavelength of light was imaged on the corresponding split detector. As the microsphere moved freely in the trap, 17 to 18 Hz oscillations in the trap initiation slide caused an oscillation of the same frequency in the vertical position of the microsphere. This oscillation was treated as real microsphere motion.

The microsphere position signals from this experiment are shown in figure 6-2. It is qualitatively clear that the persistent oscillation at approximately 17 Hz is better resolved by the small-angle refraction method than by large-angle reflection. These data were acquired at a 2 kHz sampling rate and with detector bandwidths above 700 Hz. The Fourier transform of this data, displayed in figure 6-3, quantitatively confirms what was observed in the time-series plot: Small-angle refraction improves position resolution by approximately a factor of 2. We can therefore conclude that this new method for position detection senses real microsphere motion better than its predecessor.

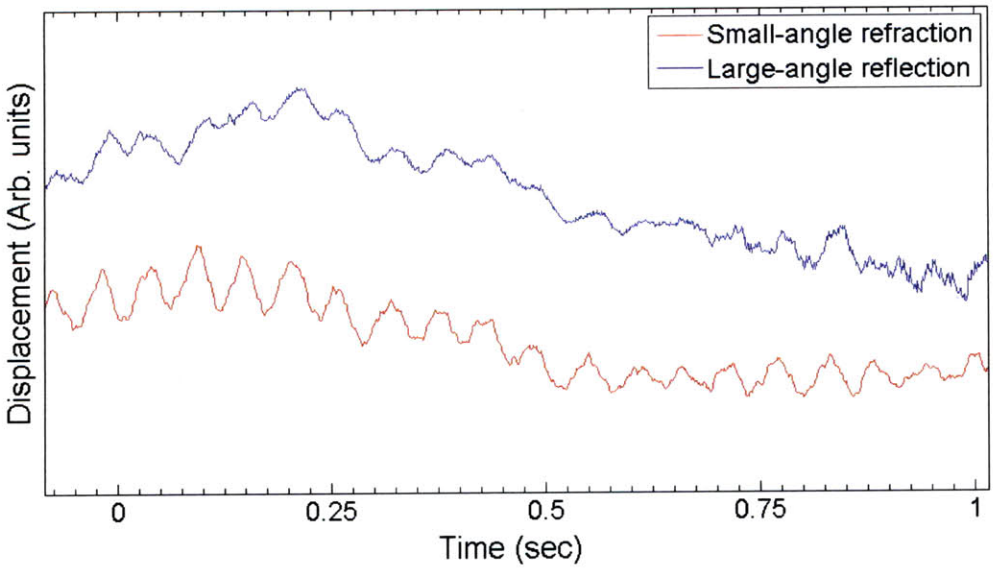

Figure 6-2: Microsphere motion induced by oscillations in the trap initiation slide. Position detection based on refracted light visibly improves resolution.

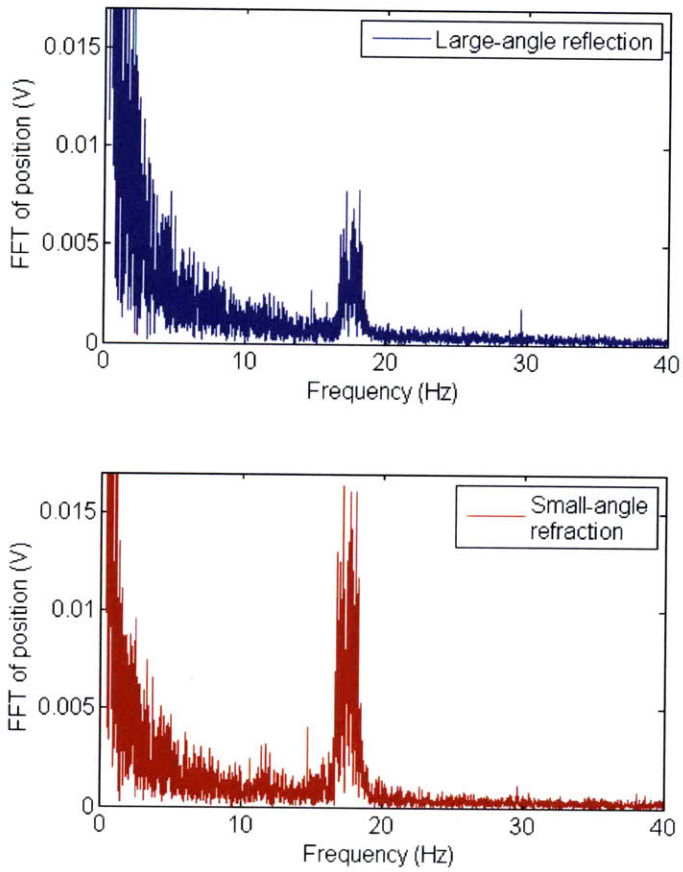

Figure 6-3: Fourier transforms of position signals obtained simultaneously confirm resolution improvement.

6.2.2 Instability induced by misshapen spheres

The instabilities observed in previous levitation experiments were caused by either real motion, spurious position detection, or some combination of the two. If the trouble was with detection, we expected the small-angle refraction method to improve stability when position stabilization was active. Conversely, the stability was expected to deteriorate with the addition of this detection method if its source was genuine microsphere motion. To determine if the stability changed, the Allan deviations for a range of measurement intervals were measured for a closed-loop single-beam trap, operated in high vacuum and with the new position detection method. Based on the resulting Allan deviation plot, shown in figure 6-4,

the instability seen in previous work (around the 10 second measurement interval) was still present and most likely dominated by real microsphere motion.

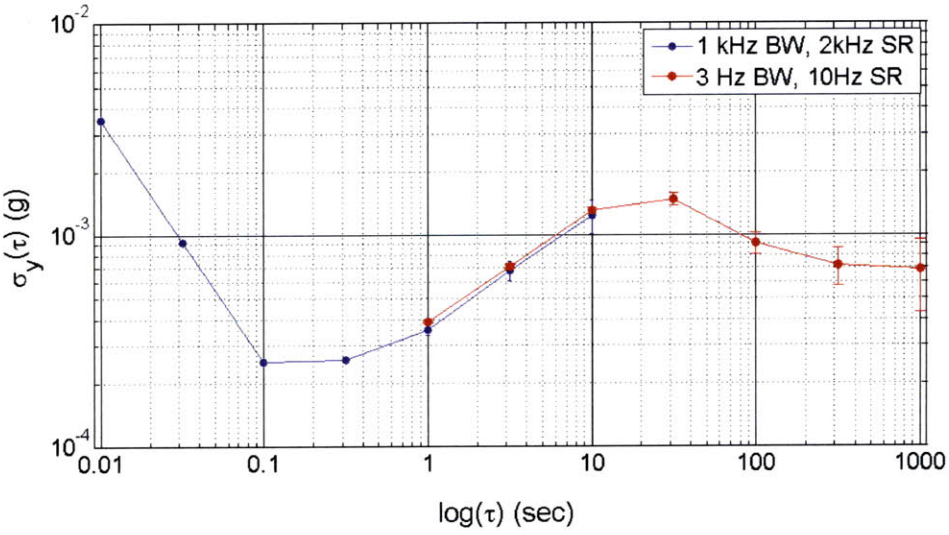

Figure 6-4: Instability in single-beam levitation persists, particularly around the 10 second measurement interval.

The rapid decrease in the Allan deviations at short averaging times resulted from the weak control of microsphere oscillations shown in figure 6-2. Without damping from air, the oscillations grew in amplitude to the point where trapping was only possible when the controller did not resist this motion. Therefore, the oscillations were not present in the power signal and did not contribute to instabilities in the Allan deviation. Recall that the position oscillations had a period of about 0.06 seconds, which is very close to the measurement interval of the minimum Allan deviation. Had these oscillations been controlled, a larger Allan deviation would have resulted at this interval. To avoid the instabilities driven by the trap initiation slide, a dual-beam trap with beams propagating over the slide was used to levitate microspheres.

6.3 Development of the dual-beam optical trap

6.3.1 Demonstration of trapping

The dual-beam optical trap used two focused, counter-propagating, horizontally oriented beams to levitate a 10 μm diameter fused silica microsphere. Recall that in a horizontal dual-beam trap, scattering forces confine the sphere in the axial direction while gradient forces balance gravity. Since the $1/e^2$ diameters of the beams was 10 μm at the waist, aligning the beams was a non-trivial task.

To facilitate beam alignment, the focusers were placed in kinematic mounts (K6X, Thorlabs), pictured in figure 6-5, which provided milli-degrees of angular resolution for pointing. These mounts were secured to 3-axis translation stages, which permitted linear position adjustments that were accurate to 2 μm. Once the angular orientations of the kinematic mounts were matched, the horizontal beams were translated to positions where they intersected the path of the vertical beam. This step helped ensure that microspheres would be successfully transferred from the vertical beam to the horizontal beams once the alignment process was completed (the microsphere hand-off procedure was described in section 5.5.3. The placement of one horizontal beam was refined iteratively in all three spatial dimensions by using the beam to eject microspheres from the vertical-beam trap with successively lower power levels. When it became possible to eject microspheres from the 50 mW vertical beam with 25 mW in the horizontal beam, the beams were aligned in the plane perpendicular to the z-axis (the xy-plane) to within 10 μm. At this point, levitated spheres were likely to be positioned within the Rayleigh range of the horizontal beam (the Rayleigh range is discussed below). This procedure was repeated with the second horizontal beam primarily to help determine its z-axis position. The second beam was then aligned relative to its counterpart by adjusting its linear position in the xy-plane to maximize the light coupled from one focuser into the other. Trapping at this stage was typically still not possible because of angular misalignments. The simplest solution was trial and error: trapping was attempted with different relative beam orientations by translating second beam in the xy-plane and then adjusting its angular position to maximize the light coupled from one focuser into the other.

Visual indicators of improvement in the alignment were very important in this process.

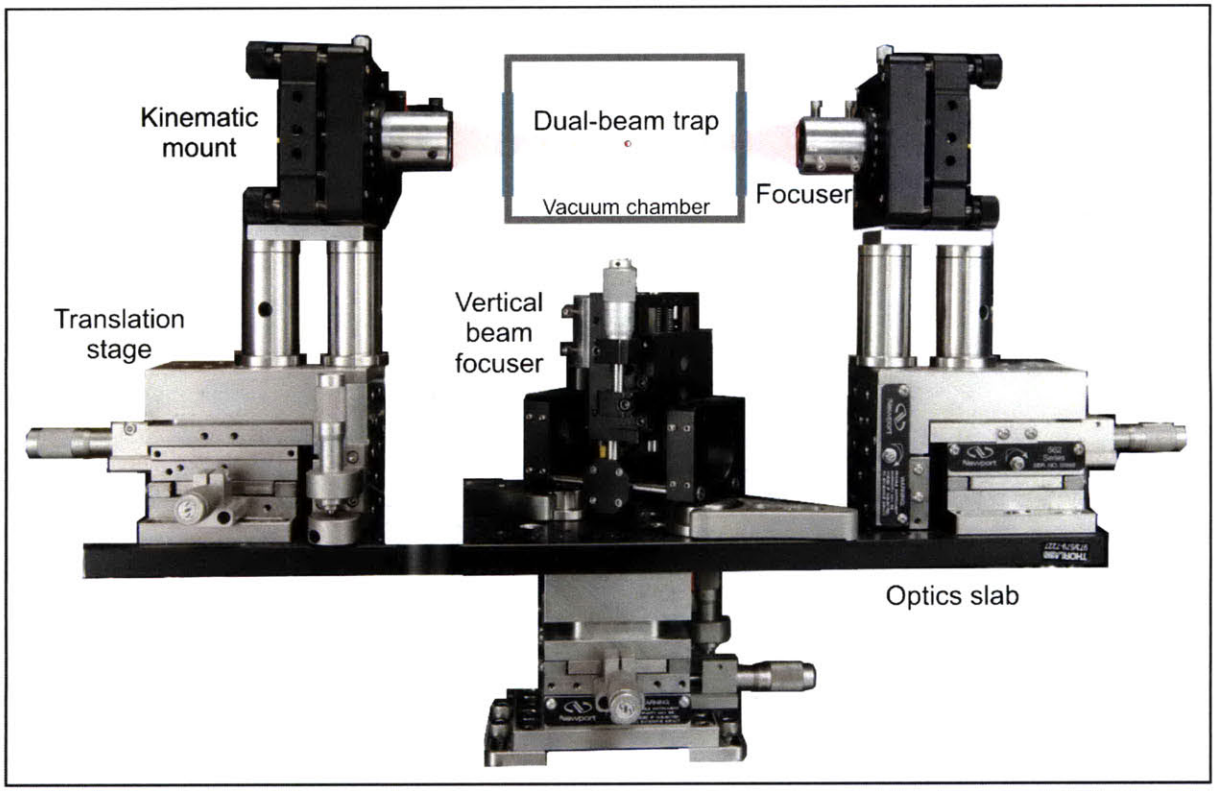

Figure 6-5: Horizontal and vertical beam focusers are mounted on the same moveable surface.

If the beams were badly misaligned, the microsphere was immediately ejected from the vertical beam during an attempt at a microsphere hand-off. Moderate misalignment, however, resulted in microspheres being initially accepted by the dual-beam trap and then lost when the power of the vertical beam was reduced. Variations in the power level at which spheres were lost also indicated a change in the alignment quality (assuming the variation could not be accounted for by differences in microsphere mass).

Following this alignment algorithm revealed that stable trapping was possible when the second focuser was positioned anywhere within a 0.25 mm^2 area in the xy-plane, centered on the axis of the other beam. The tolerance to angular misalignment is explained by the force diagram in figure 6-6, in which scattering forces resolve to expel the microsphere from the trap and gradient forces provide resistance. Such traps have been experimentally demonstrated in liquid environments, with beams emitted directly from optical fibers [23]. Separation between the foci in the z-axis also has an associated tolerance that is characterized by the Rayleigh range: the position in the z-axis where the cross-sectional area of the beam is twice the area at the waist. Beyond this position, the microsphere receives substantially less power from the beam than it would at the focus. Mathematically, the Rayleigh range is defined as

$$z_R = \frac{\pi {w_o}^2}{\lambda} \tag{6.1}$$

where w_o is the beam waist and λ is the wavelength of the laser beam. For the horizontal beams, $w_o = 5$ μm and $\lambda = 980$ nm, yielding $z_R = 96$ μm. Trapping should therefore be possible for foci separations in the vicinity of 200 μm or smaller. Experimentally, trapping was demonstrated over a change in foci separation of approximately 300 μm, though angular and xy-plane positions of the focusers were changed. The separation between foci in the z-axis is an important factor in the sensitivity of the LFA, as discussed in section 2.3. the other.

The minimum power necessary to levitate a microsphere in the dual-beam trap was 35 mW per beam, though only 95% of this power was incident on the sphere. Below this power level, the sum of the gradient forces was unable to balance the weight of the sphere. A theoretical calculation, based on the discussion in section 2.2.1, predicted that 15 mW per beam would be sufficient to levitate a microsphere weighing 1.15 nangrams—approximately

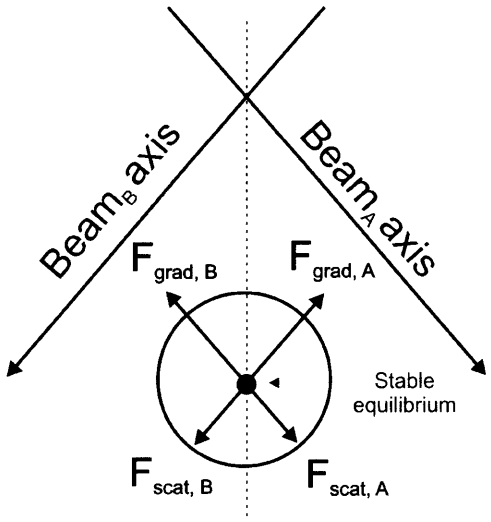

Figure 6-6: Angular misalignments of the counter-propagating beams. Trapping is possible, nevertheless.

the weight of the spheres used in these experiments. The agreement between these numbers to within a factor of $\sim$2 indicates that the beam alignment procedure provides a reliable alignment. We note, finally, that in most experiments the horizontal beams used about three times the minimum power to provide stronger confinement of microspheres.

6.3.2 Dual-beam trap in vacuum

Trapping was demonstrated in high vacuum with the dual-beam system, though only for short periods of time. When the pressure level dropped below 1 mTorr, undamped microsphere oscillations along the z-axis persisted for tens of seconds before ejecting the sphere from the trap. The source of this instability was a mild beam misalignment caused by motion of the vacuum chamber. For example, flexible vacuum hardware components, such as bellows, visibly rotated the vacuum chamber during evacuation. Since the horizontal beams passed through the windows of the chamber, they were redirected and, as a result, required constant realigning. The torquing effect was eliminated by mounting the vacuum chamber rigidly and replacing bellows with firm vacuum components. In turn, the optics were made free to move relative to the trap initiation slide by mounting them on a single 3-axis translation stage, which was shown in figure 6-5. This configuration, however, added its own mechanical instabilities because ground tremors easily coupled into the long moment arms

of the supporting slab. Unfortunately, microsphere oscillations in the modified apparatus proved to be an intractable barrier to long-term dual-beam trapping in vacuum.

To verify that the source of the oscillations was not a natural property of the trap, a sphere was levitated in air and a sinusoidal power dither was applied over a range of driving frequencies. The amplitude of the resulting position oscillation was then examined as a function of dither frequency to check for a resonance frequency in the system. An example of the position oscillation signal along with the resulting Fourier transform is shown in figure 6-7, and the amplitude response as a function of frequency is plotted in figure 6-8. The frequency of the oscillation at sub-atmospheric pressure, which was 22 Hz, clearly did not cause a resonance here. It is possible that because this experiment was done in air, the system was overdamped and resonances were suppressed. However, difficulties with vertical beam levitation in vacuum-a fairly routine procedure in previous work-corroborated the theory that mechanical instabilities were the source of these position oscillations.

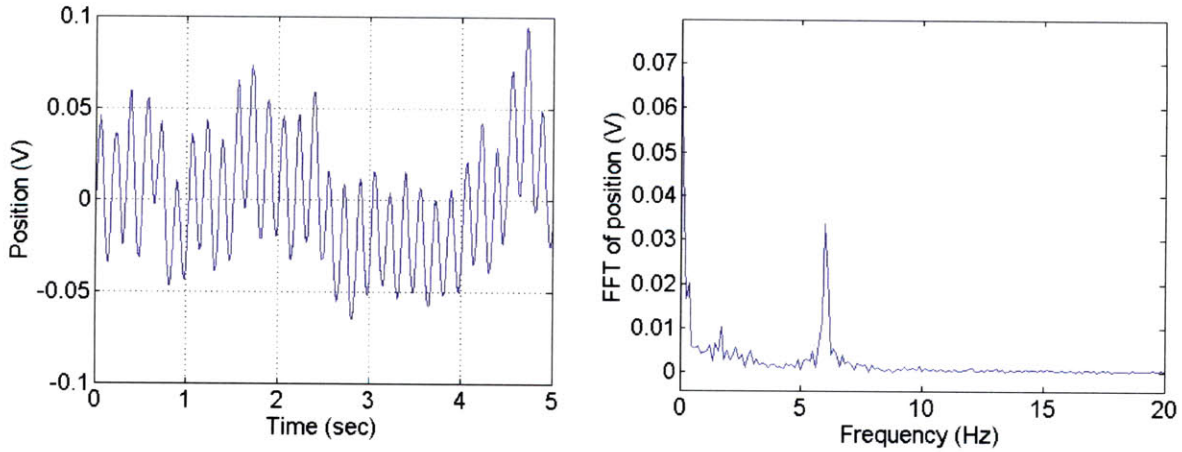

Figure 6-7: Left: 6 Hz oscillation in microsphere position in response to power oscillations at the same frequency in the horizontal beams. Right: Fourier transform of the position signal.

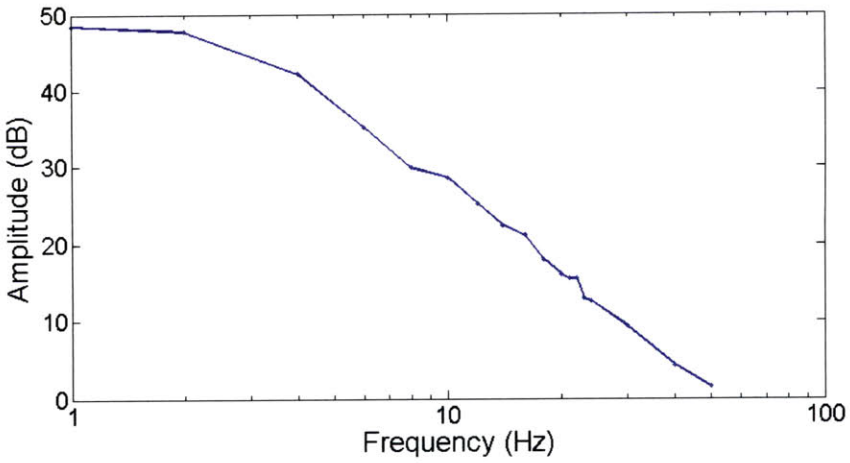

Figure 6-8: Amplitude response of the system over a range of 50 Hz. The system behaves like a double-integrator because of overdamping from air.

6.4 Proof mass confinement through optical force-rebalancing

Optical force-rebalancing in the dual-beam trap was demonstrated by using the large-angle reflection method for position measurement. Microsphere motion was measured by a split photodetector and sent to an analog PID controller; integral control eliminated undesirable stead-state position errors and derivative control helped damp persistent oscillations, particularly in vacuum. A correction signal from the controller tuned two FVOAs, which determined the power levels in each beam. Since two beam powers were being varied, there was some freedom in choosing a control algorithm. In this system, power differences were created while maintaining a constant total power between the two beams. As a result, the gradient force was constant and the coupling of transverse microsphere motion with axial motion was reduced.

The time-series plot of microsphere position, shown in figure 6-9, represents typical error signals during closed-loop trapping. Taking three standard deviations as a measure of the maximum microsphere displacement, we see that the controller confined the peak-to-peak position of the sphere to about 1 μm. The split detector signal (originally in Volts) was converted to units of length by translating the vertical beam laterally by a known amount while a sphere was trapped, and monitoring the motion with the split detector. It was found

that a 3-micron position deflection created an average error signal of 20 mV.

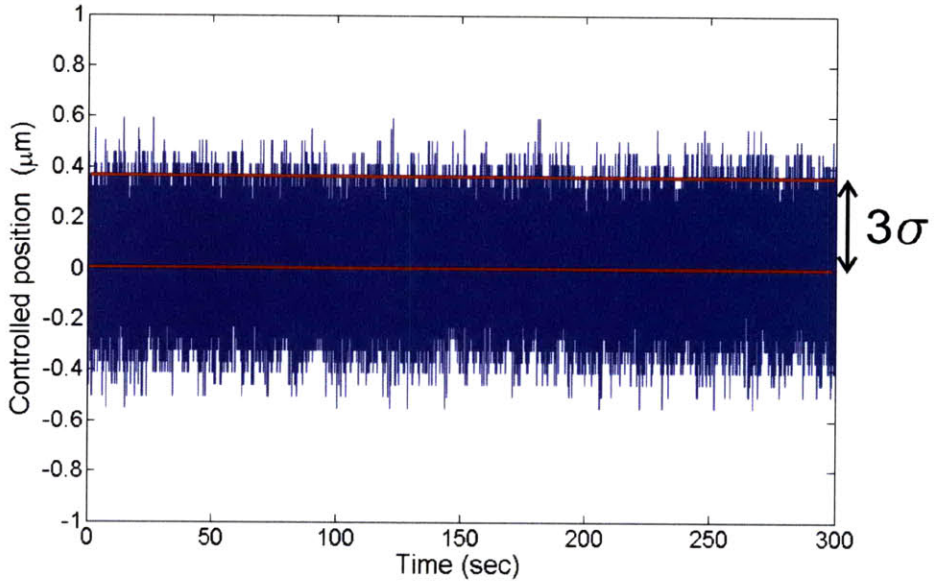

Figure 6-9: Position error signal for a stabilized microsphere. The motion is restricted to < 1 μm.

6.5 Performance Diagnostics

This section presents preliminary calculations of short-term sensitivity and bias stability for the LFA in a closed-loop, dual-beam configuration. The data used to determine these performance parameters were acquired from a trap in air because long-term trapping in vacuum was prohibitively difficult. As discussed in chapter 3, high-vacuum improves the sensitivity of the LFA by eliminating photophoretic forces and microsphere position jitter due to gas collisions.

Sensitivity and bias stability are typically quoted in units of $g/\sqrt{\text{Hz}}$ and g, respectively. The power differences between the counter-propagating beams were calibrated to gs by measuring the minimum power required for levitation with a vertically oriented beam of the same focal length and waist diameter. The minimum power, at 40 mW, was assumed to be proportional to 1 g, giving the relationship

$$\delta a = \frac{g}{40\text{mW}} \delta P \tag{6.2}$$

It is important to note that this calibration does not account for the position of the sphere along the beam axis, which can significantly alter the power necessary for levitation. In a better calibration technique, discussed conceptually in section 3.2.2, a sinusoidal variation is applied to the power of the trapping beams. The dynamics of undamped simple harmonic motion then relate displacements of the microsphere to power changes over a range of driving frequencies. Since these dynamics apply best to a microsphere in vacuum, this method could not be used effectively. Attempts were made to apply continuous calibration to microspheres im air, but drag effects were not understood well enough for this technique to be reliable.

6.5.1 Short-term sensitivity

Short-term sensitivity is a measure of how well an accelerometer resolves inertial inputs over short time scales. To determine this quantity, the power differences ΔP were sampled for one minute while microsphere position was actively stabilized in air. Since there were negligible drifts over such a short period of time, the standard deviation provided an appropriate measure of the smallest input that could have been resolved. Therefore, the resolution in gs is $\sigma_a = C\sigma_{\Delta P}$, where $C = 1g/40\text{mW}$, and σ_a and $\sigma_{\Delta P}$ are standard deviations.

Since the power measurements were actually acquired in units of Volts, namely V_1 and V_2, ΔP was determined by taking the normalized difference of V_1 and V_2 as shown in the expression

$$\text{Normalized difference} = \frac{\text{V}_1}{< \text{V}_1 >} - \frac{\text{V}_2}{< \text{V}_2 >} \tag{6.3}$$

The mean values V_1 and V_2 were proportional to the measured powers in each beam at the start of the experiment, which were both 100 mW. Therefore, ΔP = (Normalized difference)$\times$ 100mW. For the data shown in figure 6-10, $a = 26$ mg. Since the bandwdith was limited to 1 kHz, the short-term sensitivity is 822 $\mu g/\sqrt{\text{Hz}}$. A Fourier transform of the data used in this calculation revealed color in the noise processes, implying that the standard deviation was overestimating the variation in the signal. If we consider frequencies over which the noise process is fairly white, the estimate of short-term sensitivity drops to about 500 $\mu g/\sqrt{\text{Hz}}$.

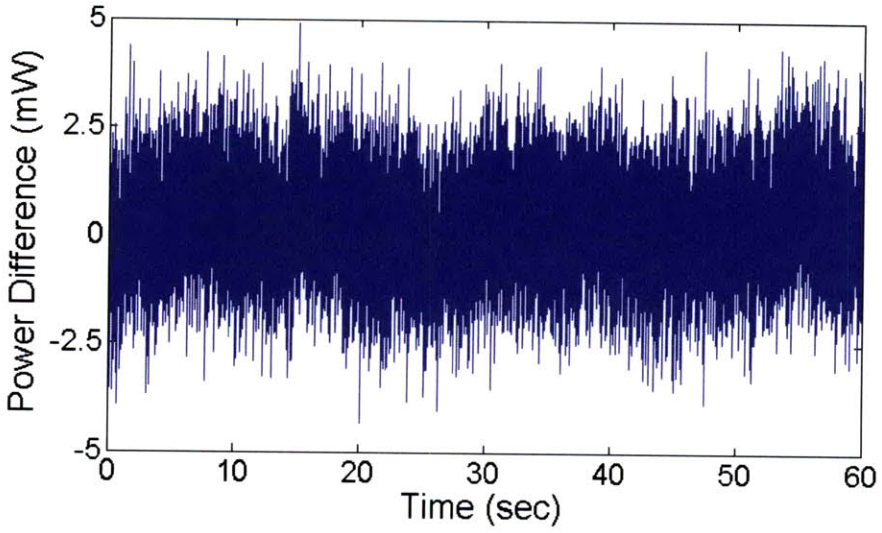

Figure 6-10: Time-series plot of data used for a short-term sensitivity calculation

6.5.2 Bias stability

The bias stability was determined by measuring of the Allan deviations of the normalized power differences during closed-loop operation. A plot of the deviations, shown in figure 6-11, used two data sets that were acquired over a span of 5 minutes (blue) and 8.5 hours (red). The minimum of this curve suggests a bias stability of 318 μg at a 300 second measurement interval, and flattening of the curve around the 1 and 10 second intervals may indicate instabilities due to microsphere shape irregularities, which were observed in previous experiments with a vertical beam trap. Additionally, the $\tau^{1/2}$ slope of the curve between the 300 and 1000 second measurement intervals indicates a random walk, which is expected over long periods of time.

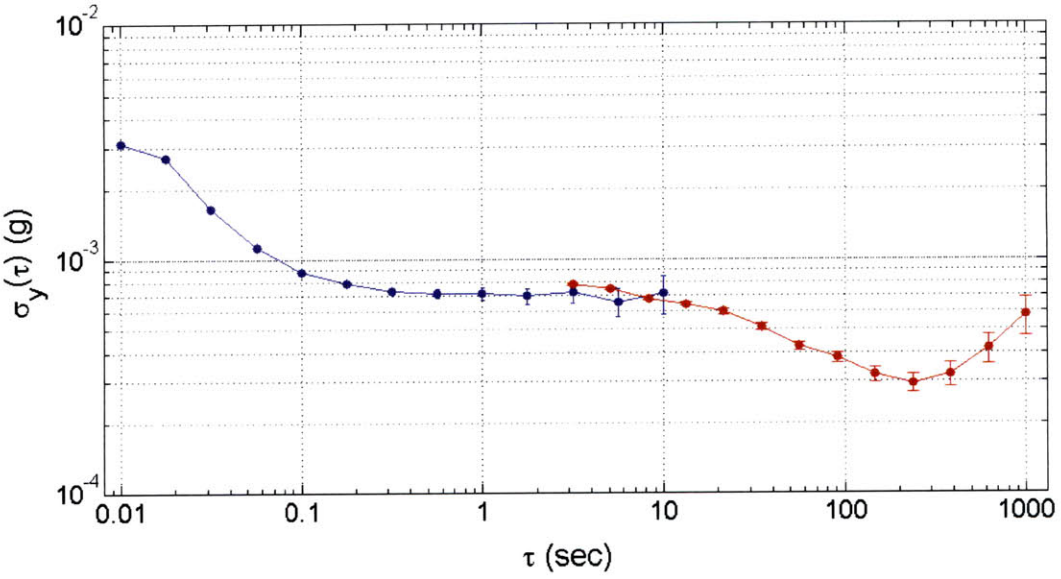

Figure 6-11: Allan deviation of the dual-beam trap over a range of measurement intervals. The minimum Allan deviation at $\tau = 300$ sets the bias stability at 318 μg

THIS PAGE INTENTIONALLY LEFT BLANK

Chapter 7

Conclusion

7.1 Summary

In this thesis, resolution of microsphere motion was improved using a new position detection method, and dual-beam trapping was demonstrated with optical force-rebalancing. While better position resolution did not eliminate instabilities caused by misshapen microspheres, it will ultimately improve sensitivity in the LFA. In addition to these demonstrations, a beam alignment algorithm was developed for the dual-beam trap. This algorithm yielded a trap whose optical forces agreed fairly well with theoretical predictions. Preliminary measurements of bias stability and short-term sensitivity were also presented to give the reader a general sense of the performance level of the current apparatus. These measurements suffered from the trapping of microspheres in air, in which gas collisions and heating effects are substantial sources of bias instability. An imprecise calibration of power measurements also added a level of uncertainty to these performance specifications. These important factors must be overcome before exact measurements can be acquired from the dual-beam trap. The rest of this chapter is devoted to recommendations for future work in the near- and long-term.

7.2 Future Work

The most pressing problem with the current apparatus is the inability to trap microspheres for long time periods in high-vacuum. Destabilizing vibrations in the moveable optics as-

sembly couple into proof mass position oscillations that grow uncontrollably. In figure 6.6, we saw that the long moment arms of the supporting slab provided some freedom of motion about a central pivot point. Since the placement of supports under the ends of each arm did not eliminate the vibrations, it may be necessary to include a translation stage with a wider platform. Trapping microspheres in vacuum is important not only for the improvement of sensitivity, but because it eases the procedure for real-time scale factor calibration. Recall that by sinusoidally dithering the power of the levitation beams, the system behaves like a driven simple harmonic oscillator. Measurements of microsphere displacement and corresponding power fluctuations, to a good approximation, completely determine the scale-factor if there is no damping from air and the driving frequency is much higher than the natural frequency of the trap. While this experiment has been successfully performed in air, demonstrations in high-vacuum and at sufficiently high frequencies (at least several hundred Hz) have yet to be done. If real-time calibration is not possible, another solution would involve tilting the apparatus by a known angle to apply a component of gravity along the sensitive axis of the accelerometer, as shown in figure 7-1. An inexpensive MEMS accelerometer could be placed on the optics platform to measure this gravity component fairly accurately. A tilting capability would also enable a formal optical force-rebalancing demonstration (in which a controlled step or ramp input is detected), as well as the measurement of scale-factor linearity, which has not be studied experimentally at this point in time. Finally, the inclusion of piezo-actuated translation stages for at least one of the horizontal trapping beams would greatly improve the quality of beam alignment. These motorized stages can provide accurate displacements to well under 1-micron.

In the far-term, the dual-beam trap would benefit from the incorporation of an illuminating beam to implement the small-angle refraction method for position detection, since this method was shown to improve resolution of real proof mass motion. Additionally, expected difficulties with cross-axis coupling of proof mass motion and automatic trap initiation will need to be addressed before the LFA becomes a deployable sensor.

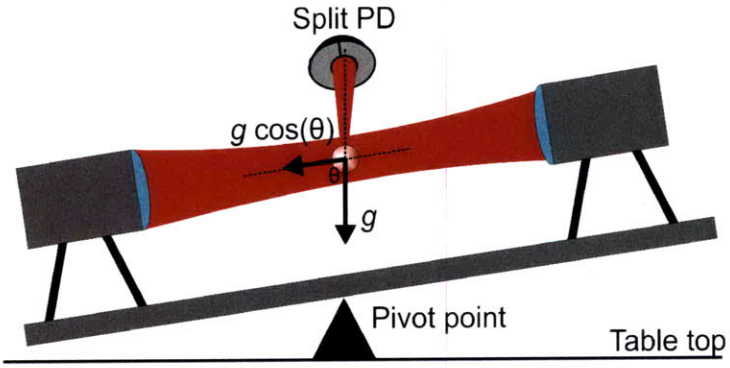

Figure 7-1: Tilting of the accelerometer sensitive axis to apply a known acceleration input along the sensitive axis.

THIS PAGE INTENTIONALLY LEFT BLANK

Appendix A

Allan Variance

The following is excerpted from the results section of reference [1]:

This statistical measure (Allan Variance) is used because the standard deviation does not converge for most signals with drifts (e.g., random walks). The Allan deviation (the square root of the Allan variance) is calculated by binning a time-domain signal into constant measurement intervals, as shown in figure A-1, and computing the standard deviation of the means of neighboring intervals. For a time series of acceleration measurements, the Allan variance $\sigma_y^2(\tau)$ for measurement interval τ is

$$\sigma_y^2(\tau) = \frac{1}{2(n-1)} \sum_i (a(t)_{i+1} - a(t)_i)^2 \tag{A.1}$$

where n is the number of bins and $a(t)_i$ is the mean of the ith bin[1].

[1]The Allan variance was developed historically for analyzing high precision clock stability.

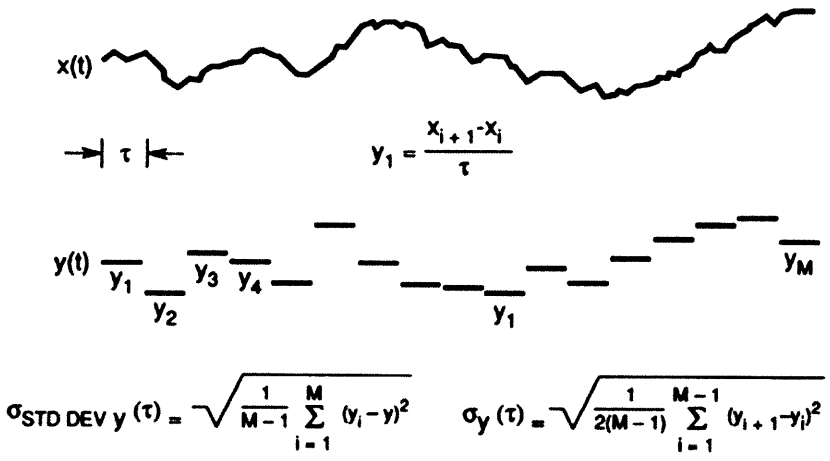

Figure A-1: Method for computing the Allan deviation of a time-domain signal.

Bibliography

[1] David L. Butts. Development of a light force accelerometer. Master's thesis, MIT, 2008.

[2] Neil Barbour and George Schmidt. Inertial sensor technology trends. *IEEE Sensors Journal*, 1(4):332–339, Dec. 2001.

[3] R. Stoner. Personal communication, Apr. 2010.

[4] Achim Peters, Keng Yeow Chung, and Steven Chu. Measurement of gravitational acceleration by dropping atoms. *Nature*, 400:849–852, Aug. 1999.

[5] David A. Mindell. *Digital Apollo: human and machine in spaceflight.* MIT Press, 2008.

[6] N. Barbour. Inertial components - past, present, and future. In *2001 AiAA Guidance, Navigation and Control Conference*, pages 1–11, 2001.

[7] A.B Tveten, A. Dandridge, C.M. Davis, and T.G. Giallorenzi. Fiber optic accelerometer. *Electronic Letters*, 16(22):854–856, Oct. 1980.

[8] A. Ashkin. *Optical Trapping and Manipulation of Neutral Particles Using Lasers.* World Scientific, 2006.

[9] A. Ashkin. Acceleration and trapping of particles by radiation pressure. *Physical Review Letters*, 24(4):156–159, Jan. 1970.

[10] H.C. van de Hulst. *Light Scattering by Small Particles.* Dover, 1981.

[11] A. Ashkin. Optical trapping and manipulation of neutral particles using lasers. *Proceedings of the National Academy of Sciences of the USA*, 94:4853–4860, May 1997.

[12] G. Roosen and C. Imbert. Optical levitation by means of two horizontal laser beams: A theoretical and experimental study. *Physics Letters*, 59A(1):6–8, Nov. 1976.

[13] A. Ashkin. Forces of a single-beam gradient laser trap on a dielectric sphere in the ray optics regime. *Biophysical Journal*, 61:569–582, Feb. 1992.

[14] Gerald Roosen. A theoretical and experimental study of the stable equilibrium positions of spheres levitated by two horizontal laser beams. *Optics Communications*, 21(1):189–194, Apr. 1977.

[15] A. Ashkin and J.M. Dziedzic. Optical levitation by radiation pressure. *Applied Physics Letters*, 19(8):283–285, Oct. 1971.

[16] A. Ashkin, J.M. Dziedzic, J.E. Bjorkholm, and Steven Chu. Observation of a single-beam gradient force optical trap for dielectric particles. *Optics Letters*, 11:288–290, May 1986.

[17] Steven Chu, L. Hollberg, J.E. Bjorkholm, Alex Cable, and A. Ashkin. Three-dimensional viscous confinement and cooling of atoms by resonance radiation pressure. *Physical Review Letters*, 55(1):48–51. July 1985.

[18] William P. Kelleher, Stephen P. Smith, and Richard E. Stoner. *Optically rebalanced accelerometer.* U. S. Patent Office, 2005. Patent number 6,867,411.

[19] A. Ashkin and J.M. Dziedzic. Feedback stabilization of optically levitated particles. *Applied Physics Letters*, 30(4):202–204, Feb. 1977.

[20] A. Ashkin and J.M. Dziedzic. *Damping of optically levitated particles by feedback and beam shaping.* U. S. Patent Office, 1978. Patent number 4,092,535.

[21] Jakob Kisbye Dreyer, Kristine Berg-Sorensen, and Lene Oddershede. Improved axial position detection in optical tweezers measurements. *Applied Optics*, 43(10):1991–1995, Apr. 2004.

[22] A. Ashkin and J.M. Dziedzic. Observation of radiation-pressure trapping of particles by alternating light beams. *Physical Review Letters*, 54(12):1245–1248, Mar. 1985.

[23] Kozo Taguch, Masaru Tanaka, and Masahiro Ikeda. Theoretical study of an optical levitation using dual beam from optical fibers inserted at an angle. *Optics Communications*, 194:67–73, July 2001.